Earthquake imprints on a lacustrine deltaic system: the Kürk Delta along the East Anatolian Fault (Turkey)

Aurélia Hubert-Ferrari[1], Meriam El-Ouahabi[2], David Garcia-Moreno[3], Ulaş Avşar[4], Sevgi Altınok[5], Sabine Schmidt[6], Nathalie Fagel[7], Namık Çağatay[8]

1. University of Liège, Department of Geography, Liège, Belgium. aurelia.ferrari@ulg.ac.be.
2. University of Cologne, Department of Geography, Germany
3. Renard Centre of Marine Geology, Ghent University. Krijgslaan 281 S.8, B-9000 Gent (Belgium).
   david.garciamoreno@UGent.be
4. King Abdullah University of Science and Technology (KAUST), Thuwal, Saudi Arabia. ulas.avsar@kaust.edu.sa
5. Osmangazi University, Engeneering Faculty, Dept. of Geology, Eskisehir, Turkey
6. University of Bordeaux, EPOC, Pessac, France.
7. University of Liège, AEGs, Department of Geology, Liège, Belgium
8. Istanbul Teknik Universitesi, Faculty of Mines, Istanbul, Turkey. Cagatay@itu.edu.tr

ABSTRACT

Deltas contain sedimentary records that are not only indicative of water level changes, but also particularly sensitive to earthquake shaking typically resulting in soft-sediment-deformation structures. The Kürk lacustrine delta lies at the south-western extremity of Lake Hazar in eastern Turkey and is adjacent to the

seismogenic East Anatolian Fault (EAF), which has generated earthquakes of magnitude 7. In this paper we have reevaluated water level changes and earthquake shaking that have affected the Kürk Delta combining geophysical data (seismic-reflection profiles and side-scan sonar), remote sensing images, historical data, onland outcrops and offshore coring. The history of water level changes provides a temporal framework for the depositional record. In addition to the commonly soft-sediment-deformation documented previously, onland outcrops reveal a record of deformation (fracturing, tilt and clastic dykes) linked to large earthquake-induced liquefactions and lateral spreading. The recurrent liquefaction structures can be used to obtain a paleoseismological record. Five event horizons were identified that could be linked to historical earthquakes occurring in the last 1000 years along the EAF. Sedimentary cores sampling the most recent subaqueous sedimentation revealed the occurrence of another type of earthquake indicator. Based on radionuclide dating (^{137}Cs and ^{210}Pb), two major sedimentary events were attributed to the 1874-1875 EAF earthquake sequence. Their sedimentological characteristics were determined by X-ray imagery, XRD, LOI, grain-size distribution and geophysical measurements. The events are interpreted to be hyperpycnal deposits linked to post-seismic sediment reworking of earthquake-triggered landslides.

Keywords Paleoseismicity, seismites, liquefaction and lateral spread, lateral spreads, hyperpycnal flow, post-seismic remobilization, East Anatolian Fault, deltaic sediments

INTRODUCTION

A lacustrine delta is a complex littoral environment due to the direct influence of both

the riverine and the lacustrine systems, and is generally characterized by high sedimentation rates. River deposits form the bulk sediments on the delta, while the lake controls the river base level and the shoreline location, which determine the shape and stratigraphy of the delta as well. As a consequence deltaic systems are good recorders of lake level changes, which could be related to past climatic changes (e.g. Stine, S., 1990; Machlus et al, 2000). Furthermore, in tectonically active areas, nearshore sedimentary environments can also contain a record of past earthquakes (e.g. Enzel et al., 2000). Delta plain sedimentary sequences contain alternations of unconsolidated water-saturated sediments with significant contrast in grain-size distributions, which makes them sensitive to cyclic ground shaking (e.g. Rodriguez Pascua et al., 2000, Montenat, 2007). In this context, the earthquake signal can be the direct expression of ground shaking, which may triggers hydroplastic deformation, shearing, liquefaction, water escape, fluidization and resuspension of the original deposits (e.g. Bachrach et al., 2001; Agnon et al., 2006; Wetzler et al., 2010). Earthquake-triggered soft-sediment-deformation structures include: flame structures, balls and pillows, intraclast breccia, convoluted bedding, billows, mixed layers, pillar and chaotic structures; these are generally called “seismites” (e.g. Seilacher, 1969; Anketell et al., 1970; Allen, 1982; El-Isa and Mustafa, 1986; Ettensohn et al., 2002; Bowman et al., 2004). However, deltas are not usual target sites for paleoseismological investigations for several reasons. First, it is difficult to unambiguously differentiate flooding or storm events from earthquake-triggered events in areas where an extensive historical earthquake catalogue does not exist. Second, deltas are complex sedimentary systems characterized by discontinuous sedimentation. Hiatuses can preclude achieving an unbiased continuous history of earthquake shaking. This is, for example, the case of some high resolution paleoseismic records of the Dead Sea Fault obtained from near shore alluvial sequences containing

sedimentary hiatuses (i.e. Ken-Tor et al., 2001).

This paper focuses on the sedimentary record of the Kürk Delta along a major active fault in Turkey, the East Anatolian Fault (EAF), which like the Dead Sea Fault (DSF) and the North Anatolian Fault (NAF), has an extensive historical earthquake catalogue exists (Ambraseys, 1989; Guidoboni et al., 1994; Ambraseys and Finkel, 1995; Ambraseys and Melville, 1995; Ambraseys, 2009) that can be used to understand the response of a given sedimentary system to the documented shocks. Hempton and Dewey (1983) first documented earthquake-induced deformational structures only in onland sedimentary sections through the Kürk Delta. A complementary study is presented here to more fully characterize the earthquake signal in the deltaic system by combining terrestrial and subaqueous records and by linking the sedimentary disturbances to the historical earthquake record. The onland archive exposed an earthquake-related imprint different from the one documented by Hempton and Dewey (1983). The offshore archive allows a focus on earthquake-related sedimentation processes on the subaqueous delta, which revealed another kind of earthquake fingerprint.

In order to work out the earthquake impact on the delta, the 1874-1875 EAF ruptures are first reevaluated by using new seismic reflection data. A reassessment of water level changes is also provided combining remote sensing images, historical and geophysical data and provides the temporal framework used here. Onshore exposures across the delta were investigated to identify lithological changes related to lake level changes and earthquake disturbances so that the seismic history of the East Antolian Fault could be reconstructed over the last 1200 years. Finally, the impact of earthquake shaking on the

structure, morphology and sedimentology of the subaqueous delta is assessed using seismic reflection data and four short cores. We used ^{137}Cs-^{210}Pb radionuclides to identify sedimentological changes related to the AD 1874-1875 EAF earthquakes. The significance of the different earthquake fingerprints is then finally discussed.

SETTING

Tectonic and paleoseismological background

The Kürk Delta is located at the south-western extremity of Lake Hazar, which occupies a complex pull-apart basin (Garcia-Moreno et al., 2010) along the central part of the EAF. The EAF is a major 600 km-long continental strike-slip fault located in eastern Turkey (Şaroğlu et al, 1992; Yönlü et al., 2013; Duman and Emre, 2013). It accommodates, together with the NAF, the westward extrusion of the Anatolian plate (ca. 21 mm/yr) away from the Arabia-Eurasia Collision Zone (Fig. 1; Reilinger et al., 2006). The EAF is a seismically active fault (Bulut et al., 2012) with an average slip-rate of 11 mm/yr and a total displacement of about 20 km (Şaroğlu et al., 1992; Reilinger et al, 2006; Hubert-Ferrari et al., 2008). The expression of the EAF in the Hazar Basin comprises a Master Fault (MF in Fig. 1) connecting the sidewall faults of an ancient pull-apart basin (Garcia-Moreno et al., 2010). The Master Fault crosses the lake from its northeastern to its southwestern corners, and was called the Havri Fault in Çetin et al. (2003). The large secondary sidewall faults are the Southern Gezin Fault, which bounds the steep southern edge of the lake, the North-western Sivrice Fault at the WSW extremity of the lake, and the Northern Fault bounding the deep subaqueous Hazar Basin to the North (Fig. 1).

The EAF displays a long record of historical earthquakes with moment magnitudes greater than 7 (Ambraseys and Finkel, 1995; Ambraseys, 1989; Guidoboni et al., 1994; Ambraseys and Melville, 1995). In its central part around Lake Hazar, the most historical earthquakes occurred in 1874 and 1875. On 3 May 1874, a large M>7 earthquake struck the region (Ambraseys, 1989) and was potentially associated with a 130 km-long rupture along the main strand of the EAF (Garcia-Moreno et al., 2010). According to Ambraseys (1989), most of the villages around the lake were destroyed, the ones along the shore were abandoned, and large landslides and liquefaction features occurred. The southern side of the lake was uplifted by 1 to 2 m along a length of about 45 km, probably due to vertical motion along this part of the fault rupture. As a result the lake level rose triggering inundations (Ambraseys, 1989). A major second shock occurred on 27 March 1875, with a magnitude estimate of 6.7 (Ambraseys and Jackson, 1998). Ambraseys (1989) stated that it affected exactly the same area as the 1874 earthquake, with more damage along the southern lake shore. The lake outlet rose again by 2 m, and the villages along the lakeshores were inundated and abandoned. Garcia-Moreno et al. (2010) proposed that the AD 1875 earthquake ruptured the Gezin Fault that has a normal component (Fig. 1). A recent paleoseismic offset attributed to the 19th sequence was also documented along this fault (Çetin et al., 2003). The AD 1789 earthquake affected mostly the area just east of Lake Hazar. The shock was inferred to have a magnitude greater than 7 because of widespread destructions in a radius of 75 km within which 51000 people were killed (Ambraseys, 1989). An antecedent event was identified along the Southern Gezin Fault, 4 km to the North-east of Lake Hazar in paleoseimic trenches: it occurred soon after AD 1420, and might correspond to the 28th March 1513 historical earthquake of magnitude M≥7.4 according to Çetin et al. (2003). Ambraseys (1989) estimated that the 1513 earthquake destroyed an area extending over

at least 340 km but he located its epicenter ~300 km to the South-west of Lake Hazar. So it is improbable if that earthquake ruptured the Southern Gezin Fault . In addition to this paleoearthquake, two antecedent large historical earthquakes (M≥7) were reported. In AD 1285, a damaging earthquake occurred in Malatya, ~85 km from Lake Hazar and may be related to an earthquake on the EAF (Ambraseys, 2009). The M≥7 AD 995 event was a destructive earthquake that totally destroyed Sivrice (Copik), as well as other cities more to the North-east along the EAF (Ambraseys and Jackson, 1998; Ambraseys, 2009). Finally two last paleoearthquakes were recorded in a paleoseimic trenches east of Lake Hazar (Çetin et al., 2003) and would have occurred between AD 130 and AD 450.

The Kürk Delta displays a range of sedimentary structures that were attributed to past large earthquakes along the EAF by Hempton and Dewey (1983) who documented the occurrence of seismites or earthquake-induced deformational features in sedimentary sections. The sedimentary sections were located on the Kürk Delta and the adjacent delta to the South-east of the Sivrice city (Fig. 2) and were composed of (1) a lacustrine facies with interbedded clay, silt and fine-grained sand in the lower half, and (2) a fluvial facies with clast supported gravels and sands in the upper half (Hempton et al., 1983). The deformation features were flat lying and were mostly composed of ball and pillow and flame structures of different sizes at the contact between fine-grained sand and clayey silt (Hempton and Deweys, 1983). These deformational structures are similar to seismites identified in the Dead Sea area (Ken-Tor et al., 2001; Agnon et al., 2006). In 2.5 m high outcrops, the authors distinguished five distinct horizons of soft-sediment-deformation structures with different thickness and spaced at irregular intervals. These seismites were formed predominantly by liquefaction or by

hydroplastic deformation due to cyclic loading, and demonstrate that the sediments of the Kürk Delta recorded past earthquake-generating ruptures of the EAF.

Lake basin characteristics

Lake Hazar is 25 km-long, 7 km-wide and 216 m-deep, and is mainly fed by the Kurk River, which drains a large area (76 km^2; Fig. 1) composed of terrains of the Cenomanian Yüksekova Melange (gabbros, basalts, andesites and dacites dykes) and the Middle Eocene Maden Melange (volcanic and sedimentary formations) related to the closing of the Tethys Ocean (Şengör and Yilmaz, 1981). It provides with the adjacent river near Sivrice the most important sediment load (80 000 tons of clay and silt each year) to the lake (Şen and Topkaya, 1997; Şen et al., 2007), and has built a large delta at the southwestern end of the lake (Figs 1 and 2). Peak flows occur during spring linked to snow melt and precipitation, and the river flow is very low during summer (Günek and Yiğit, 1995; Şen and Topkaya, 1997). Other rivers are ephemeral. After 1957, the Behrimaz River has provided more than 60 % of the water inflow (Şen and Topkaya, 1997). This river is an anthropic capture at the North-Eastern extremity of the lake through the former outflow (Fig. 1; Günek and Yiğit, 1995; Şen and Topkaya, 1997). The Kürk River is presently providing ~15% of the water inflow (i.e. 6 $x10^6$ m^3/yr, Sen et al., 2007).

Significant water level changes in Lake Hazar were documented using high-resolution seismic profiles, sediment cores (Eriş, 2013) and historical data (Yiğit 1995; Tonbul and Yiğit, 1995; Aygün, 2006, 2008). A maximum lowstand level (-73m) occurred during the Late Glacial-Holocene transition (Eriş, 2013). The beginning of the Holocene was associated with a large transgression and is responsible for the largest delta-building

phase at the mouth of the Kürk River (Delta 1 in Eriş (2013) . Two younger superimposed delta complexes, labeled Delta 3 and 2 in Eris (2013), further attest that significant water-level changes occurred during the Holocene. The youngest delta 3 overlies a fluvial facies, which was sampled by a sedimentary core, 1.65m below the water/sediment interface presently below 15.5m water depth. Eriş (2013) inferred a link to the 3000 BP dry Bronze Age crisis documented around the Mediterranean and particularly in Lake Van located 150 km to the northeast (Lemcke and Sturm, 1997; Wick et al., 2003). The topset beds of the youngest Delta 3 are eroded suggesting the occurrence of a recent lowstand, which age was not constrained by Eriş (2013). Historical data provide complementary data (Fig. 3). A sunken walled Armenian monastery along the lake southern shore named Surp Nshan, Cowk or Dzovk of Cowa was inhabited by Armenians from the 12th to the 18th Century (Yiğit 1995; Aygün, 2006, 2008). It attested for the occurrence of a 6th century long lowstand. Starting around 1795 after the AD 1789 earthquake, the water rose and triggered the abandonment of the settlement around 1830 (Tonbul and Yiğit, 1995). Water level reached its highest possible level, 1253 m a.s.l, just after the AD 1874-1875 earthquakes, and overflowed to the Tigris River. A large 30m lake level rise thus occurred during the 19th century. The lake stayed near its maximum level during the first half of the 20th Century with especially high levels in 1911 and 1953 when heavy rainfall occurred (Tonbul and Yiğit, 1995). In the 1970's a 10 m water drop took place due to water pumping by power plants put in operation in 1957 and 1967 for irrigation of the Elazig plain to the north (Tonbul and Yiğit, 1995). The largest 2.4 m drop occurred in 1973, when 182.4 million m^3 of water were pumped and low rainfall occurred (Tonbul and Yiğit, 1995). Since 1974, the activity of power plants decreased, and the lake level stabilized around 1238 m a.s.l. Since 1980, the lake level has only slightly increased; it has stayed around

or below 1240 m a.s.l. with significant metric variations linked to seasonal and annual rainfall variability. There is presently no lake outflow.

MATERIALS AND METHODS

In a first step, onland and subaqueous investigations were combined in order to reevaluate past water level changes and to provide an adequate sedimentological and chronological framework. Then the impact of earthquake shaking and its imprint on the Kürk Delta were assessed.

Onland investigations

The onland study rested upon the analysis of remote sensing images and stratigraphic sections. To highlight the impact of lake level changes on the Kürk Delta, the following remote sensing data were combined: topographic maps obtained using aerial photography taken in 1952 and 1955, a Corona image dating from 1960, a SPOT image from 2005 and a Google Earth image from 2010. Sedimentary deposits in the Kürk Delta were prospected using the natural outcrops created by fluvial incision as a result of the most recent lake level drop. This provided information about the shoreline location during the 19th Century highstand and human induced alterations. It also confirmed the occurrence of the structurally deformed layers already documented by Hempton and Dewey (1983). Our study focused, in particular, on one outcrop located along the main northern channel of the Kürk River 650 m westward of the present shoreline (N38^{o}27.855; E39^{o}17.443; Figs 2 and 5). The studied riser was cleaned down to the present alluvial channel, and sections of 2.5 m high and several meters long was logged and described. For that purpose, a 1 m × 1 m string grid was used on the trench walls with a coordinate system whose origin lay at the southwestern base of the trench.

On sections, earthquake-related deformations and the facies changes associated with the water level variations were investigated. In the following, the section presenting the largest structural deformation was described and interpreted. Others were used to confirm the interpretation.

Subaqueous investigations

Seismic survey and side-scan sonar

The Geophysical data consisted of high-resolution seismic-reflection profiles and side-scan sonar data acquired in 2007. Two seismic acquisition systems were used. The first system was an Innomar SES2000-Compact Sub-bottom Profiler, operated by ITU-EMCOL (Turkey). The second one, operated by the University of Gent (Belgium), was a "centipede" multi- electrode sparker with a 300 J acoustic source (main frequency of 400 – 1500 Hz), and a 10- hydrophones single-channel streamer, with an active length of 2.7 m. A grid was acquired with the Innomar System and with the sparker system. The seismic data allowed investigation, in particular, of the delta stratigraphy in relation to recent lowstands/highstands, the fault ruptures induced by the AD 1874-1875 earthquakes, and the whole delta morphology influenced by earthquake shakings. We particularly seek to identify the historical 12th-18th Century lowstand not previously docemented in seismic lines (Eriş, 2013), and to confirm the lowstand amplitude with respect to the present level. The side-scan sonar survey was operated by the University of Gent (Belgium) using a KLEIN 3000 device that simultaneously recorded in two frequency bands of 100 and 500 kHz. Towfish depth regulation was done manually. Side-scan sonar data of the sunken Armenian settlement combined with seismic profils were used to quantitatively reevaluate the 19th Century lake level changes presently based only historical sources (Tonbul and Yiğit, 1995)

Sediment cores

Four short sediment cores, namely H002, H003, H005 and H006, sampled the first meter of the lacustrine sediments on the delta. They were collected with an modified UWITEC gravity corer in 2006 within the framework of the Seismic Cycle project (Hubert-Ferrari et al., 2007). Different types of analyses were performed to characterize the continuous background sedimentation, its relation to the lake level variations and rapidly deposited layers potentially related to earthquakes. A stratigraphic log of all of the cores was first established based on X-ray imagery. Magnetic susceptibility and density data were acquired along the cores at 5-mm resolution, using the Geotek multi-sensor core logger (MSCL) of Rhodes Island University (USA). Grain-size distribution analyses were performed on the H002 and H005 cores using a Malvern Mastersizer. To constrain compositional changes, bulk mineralogy analyses were done using X-ray diffraction (XRD) on the H003 and H005 cores. Organic matter and carbonate contents along the cores were determined with the loss-on-ignition (LOI) method. The age of the sedimentary record was estimated using ^{137}Cs and ^{210}Pb short-lived radionuclides in H002, H005 and H006 cores. Measurements were performed by gamma spectrometer on samples at depths of 0-1 cm, 3-4 cm, 8-9 cm, 14-15 cm, 20-22 cm and 30-32 cm. Additional deeper levels were measured on H002, which shows the highest sedimentation rate. Excess ^{210}Pb was calculated as the difference between total ^{210}Pb and ^{226}Ra activities. The sedimentation rate was calculated based on the decrease in excess ^{210}Pb, by assuming a Constant Flux/Constant Sedimentation (CFCS) model (Goldberg, 1963).

TECTONIC AND WATER LEVEL FRAMEWORK

Recent Surface Rupture

Garcia-Moreno et al. (2010) established an accurate fault map across Lake Hazar using the same sparker seismic-reflection data (Fig. 1). The additional Innomar seismic-profiles profiles presented here documented the occurrence of the recent surface breaks along the faults mapped. The scarps were detected along two distinct fault segments, the main fault strand and the NW Sivrice Fault (Fig. 4).

Near the Kilise Island (or Gölcük Adasi) and the sunken Armenian settlement (Figs 1 and 2), the Innomar seismic-reflection profile in Figs 4D, 4E, 4F showed a 2.5 m high scarp across the slope of the promontory crossed by the EAF. To the south of the scarp the uppermost strata was wraped. The occurrence of a large surface scarp associated with a near surface deformation along a mapped active fault support its association with the AD 1874-1875 shocks as these earthquakes were the largest and the most recent ones. The observed offset may not reflect the coseismic vertical deformation for two reasons. First, the EAF was running at an angle across a slope with significant small-scale topography (Fig. 2) and a large coseismic horizontal offset may be partly responsible for the observed scarp. Second, the scarp was discontinuous and could not be found on the other seismic profiles. The vertical offset documented on a particular spot of the EAF is thus probably not representative of the earthquake slip.

In front of the Kürk Delta, the Innomar seismic-seflection profile in Figs 4A, 4B and 4C shows another marked deformation of the lake floor. The apparent offset reaches 3 m and is associated with a warping of the sedimentary cover on the ENE side of the scarp.

The profile showed an incomplete picture because of gas blanking, which occurred on most seismic profiles at the foot of the Kürk Delta. The surface scarp is inferred to be related to the AD 1874-1875 sequence, because it occurred along the mapped NW Sivrice fault splay and was associated with a shallow deformation zone. The vertical offset is visible only on the line displayed in Fig. 4A, so it could be associated with a small-scale local push-up structure.

The geophysical data thus implies that both the EAF and the NW Sivrice fault ruptured during the 19th Century. The large magnitude earthquakes responsible for these ruptures must have strongly impacted the adjacent Kürk Delta.

Recent water level changes

The anthropic 1970's water level fall (Fig. 3) has strongly impacted the Kürk Delta because of its very flat surface. During the 50's, topographic data show that large parts of the delta were covered by swamps and a deciduous tree cover (Fig. 5). Flooding by the Kürk River or by natural lake level variations would have impeded any significant development on the Delta plain. At that time all the infrastructures including the main road to Sivrice and the 1930's railway to Diyarbakır were located along the fan head at the limit of thick fluvial gravelly packages characterized by a white hue in the Corona image. Investigated outcrops (Fig. 2) adjacent to the railway indicated that near-surface sediments were composed of fine sandy silt with centimetric wavy and laminar bedding indicating nearshore facies. The railway was therefore located near the shoreline at the beginning of the 20th Century. Tonbul and Yiğit (1995) indicate that in 1953, the lake reached its highest possible level and that the railway was partly flooded. Investigated

outcrops east of the railway indicated that significant sediment dumping and infilling occurred on the top surface probably after 1953 to protect the infrastructures. In addition, the 1960 Corona image has shown that the main road to Sivrice that was located near the railways had been abandoned. A new road was constructed on the dumped sediments further east (Fig. 5). More recent anthropic water level falls resulted in enlargement of the subaerial delta plain and in flowing of the Kürk River along two branches, with active channels incised 2-3 m below the plain. Because of the river incision, most of the delta plain was preserved from flooding. Its top surface is inferred to be a non-depositional surface subjected mostly to erosion by rainfall and runoff. The newly available land has been occupied by improved or new road infrastructures, factories, agricultural fields, gravel and clay extraction, and the growing city of Sivrice.

Geophysical data were used to reevaluate the 19th Century highstand and the antecedent lowstand. The 12th-18th Century lowstand subaerial surface was identified as high reflective surface in seismic reflection profiles near the drown settlement (Figs 4D and 6B) and as an unconformity in profiles on the Kürk Delta (Fig. 7) and on secondary shallow deltas on the northern coast (see location in Fig. 2). The surface is presently overlain by a 1.25 to 0.50 m thick transgressive mud drape deposited during the subsequent highstand (layer A in seismic lines in Figs 6 and 7). The extent of erosional unconformity was be mapped until a water depth of about -22 m. The geophysical data thus confirm the magnitude (i.e 30 m) of the waterlevel increase during the 19th century inferred from historical data (Fig. 3). Geophysical data around the underwater Armenian settlement located to the southwest of the Kilise Island provide further information (Figs. 1, 2 and 6A). The side-scan images particularly showed the ~5 m high curtain wall surrounding the 10 m high gate towers (Fig. 6A), which still stand

above the lake surface. A second lower protective wall structure was imaged running to the SW of the first wall. The two different walls were built only to the south, where the connection to the land existed, indicating that the lake was used as a natural defense (Aygün, 2008). The seismic profile crossing the southern fortified wall allowed an accurate determination of the past water depth, which could not be obtained by the side-scan sonar because it was manually towed (Fig. 6B). The second fortified wall is presently submerged under 9 m of water. The lowstand subaerial surface is inferred to be the highly reflective horizon appearing 1m below the water sediment interface in the seismic profiles. Hence considering the 1 m thick sedimentary deposit since the 19th Century and the 10 m 1970's water drop, the wall drowning would have started when the water level reached 1228 m a.s.l. triggering abandonment of the settlement. Our data thus agree with historical data suggesting a rapid lake level rise followed by the abandonment of the settlement around AD 1830 (Yiğit, 1995; Fig. 3).

EARTHQUAKE IMPACT VISIBLE ON THE ONLAND DELTA PLAIN

The onland study provided a record of past water level changes and earthquake shaking. The studied section, a natural terrace riser of the main northern strand of the Kürk River, strikes NE-SW (Figs 2 and 5). It was located along the lake shore in the 1950's (Fig. 5), but is presently onland because of the 1970's lowstand. It revealed a sequence of silty clay layers (*SC*), silty clay layers with fine sand (*SCs*), sand sheets (S) and channels filled by sands (*Ch-S*) or by gravels (*Ch-G*), which were disturbed by fracturing and clastic dykes. The stratigraphy provided a chronological framework for the observed structural disturbances. Fig. 8B presents the log of the wall, while Fig. 8A presents the overall photograph of the wall and also the details of the dykes (*Dy*) and

fractures disturbing the stratigraphy.

Stratigraphy linked to past water level changes.

The outcrop can be better described from top to bottom by focusing on its southwestern part (left on Fig.8B), where the stratigraphy was nearly undisturbed. The different deltaic sedimentary facies were identified as in Dunne and Hempton (1984) and Hempton et al. (1983): (1) fluvial deposits with channel and bars, sheetflow and overbank deposits; (2) shore deposits composed of well sorted sand or pebbly gravel; (3) nearshore facies with thinly interbedded clay, silt and sand; (4) lacustrine facies of the prodelta comprising mostly massive clay. The main criteria to distinguish the different facies were grain-size and sedimentary structures.

Six different units were logged (Fig. 8B). Below the top erosional surface, two very different units were found. The first unit *U1* is composed of a layer of massive dark brown silty clay (*SC1)* overlying a silty clay layer interbedded with very fine sand layers *SCs1*. The massive silty clay *(SC)* facies is identical to the present lacustrine mud drape sampled by sedimentary cores and thus indicates a typical lacustrine environment. The silty clay facies with fine sand *(SCs)* indicates a more near shore facies. The second unit U_{Mel} is composed of a mix of pebbles, gravels and mud-clasts of different sizes and orientations in a silty clay to granulated matrix without structure; it formed a mélange of different materials mixed, crushed and fractured. This chaotic mélange also contains ripped blocks of the lacustrine sediments, with their original stratigraphy included in between more intensely deformed zones. This unit appeared at the horizontal distance H: 1.30m, and fills different dyke funnel shapes labeled ***Dy2*** to ***Dy7***. Its thickness dramatically increased toward the NE side of the outcrop. Unit U_{Mel} overlaid different

sedimentary units and its base is diachronic. The unit *U2* is comprised of: three silty clay layers with fine sand *(SCs2, SCs3, SCs4)*, two channels filled with sand *(Ch-S1, Ch-S2)* and massive sand layers (*S1, S2, S3*). The SCs layers are interpreted as overbank deposits, the channels correspond to a channel and bar facies, and S layers would have been deposited from sheet floods. Unit *U2* would thus have been formed in a braided stream on the delta plain. The facies change between the fluvial unit *U2* and the lacustrine unit *U1* indicated a water level increase. Unit *U*3 was composed of two coarse-grained channel-form subunits *(Ch-G1, Ch-G2)*. The top subunit *Ch-G1* was associated with a large basal erosion surface and was composed of gravel. The bottom subunit *Ch-G2* showed very poorly sorted gravel with matrix contents from medium sand to granule. Unit *U3* is interpreted as a typical delta plain deposit in a subaerial braided stream; it would be located farther inland than unit *U2*. The top of unit *U4* is composed of brown to grey fine sand with coarsening upward fine silty clay layers (*SCs5*) and its lower part comprises an alternation of brown to greyish silty clay and fine to very fine well sorted sand with wavy contacts (*SCs6*). The two sequences were separated by a distinctive convoluted silty clay layer in the middle (*SC2*). The fine grain unit *U4* is a typical lacustrine nearshore facies. The upward increase in grain-size in *U4* indicates a water level decrease that led to subaerial exposure and the deposition of the coarse grained unit *U3*. The basal unit *U5* is a coarse sand layer with no clay or silt (*S4*). Because only a few cm were visible, the origin of this deposit was unclear: it may be associated with a braided system on the deltaic plain or with the foreset beds of the delta front.

The facies changes observed in the outcrop can be directly related to the lake level changes presented before. The fine grained lacustrine unit *U1* would have been

deposited during the high water level that prevailed from the 19th Century to the 1950's (Fig. 3). The coarse grained delta plain fluvial facies *U2* and *U3* indicates a relatively stable low lake level, i.e the 12th-18th Century lowstand indicated by the occupation of the Armenian settlement on the southern lake shore. The transition to the fine grained unit *U4* at about 1.6m below the surface suggests an earlier highstand corresponding to the youngest Delta 3 complex (Fig. 7;–Eriş, 2013). Hempton et al. (1983) also documented this fluvial-lacustrine transition at 1.45 to 1.55 m below the surface in sections (see the location in Figs 2 and 4). The wide extent of this major stratigraphic change further confirms the occurrence of a highstand prevailing before the settling of the Armenian Monastery.

History of Deformation

In addition to the earthquake-induced soft-sediment-deformations documented in the Kürk deltaic sequence by Hempton and Dewey (1983), the studied outcrop showed extensive structural disturbances (dyking) and associated fractures (Fig. 8) with a deformation increasing toward the NE side of the outcrop. Between H: 0 m and 4 m, several fractures slightly displace the stratigraphic units revealed in the walls of the trench, with a general down to the south displacement (Fig. 8B). Between H: 3 m and 8.5 m, dykes and structural disturbances strongly disrupt the stratigraphy (Fig. 8A). From H: 2.5 m to 5.7m, the first meter of the outcrop is structureless, forming the U_{Mel} chaotic mélange that is found at progressively lower layers until H: 7.3m. To the north-east of the mapped section, the whole outcrop is completely disrupted and composed of U_{Mel}.

The following paragraphs described the different structures from SW to NE in more detail in order to constrain the different deformation phases and the location of the associated event horizons (Fig. 8B). An event horizon represents the delta surface at the time of the event that triggered the observed structural disturbances and the associated brittle deformation. That is, the top of the strongly convoluted layer *SC2* in the middle of the unit *U4* would represent such an event horizon, named here **Ev5**. Other event horizons were identified based on fractures terminations and changes in thickness or deformation related to fracturing and dyking.

The outcrop first displays an antithetic set of fractures, labeled ***F1*** and ***F2***. ***F2*** offsets the boundary between the units *U3* and *U4*, and terminates there. It is associated with a change in thickness of the layer *Ch-G2* (unit *U3*). An event horizon, labeled **Ev4** is thus located at the transition between *U3* and *U4*. ***F1*** cross-cuts ***F2***, its activation was thus posterior. This fracture ends in the layer *SCs3* in *U2*. Its termination suggests that an event, **Ev3**, occurred during the deposition of this layer. About 115 cm away from ***F2***, fracture system ***F3*** forms a unique discontinuity at depth that splays at the top of *U3* into three different branches, labeled ***F3a*** to ***F3c***. ***F3c*** ends in the structureless mélange; its termination and the associated change in thickness of the *S2 in U2* layer confirms that the **Ev3** level is an event horizon. ***F3a*** is posterior as it offsets the horizon **Ev3,** but it cannot be traced in the mélange. ***F3b*** deforms the surface at H: 2.8 m and separates the well-stratified part of the outcrop from the structureless mélange. The contact of U_{Mel} with the lacustrine sediment South-west of ***F3b*** is thus the most recent event horizon. The event at the outcrop top is labeled **Ev1.** Layer *Ch-S1* in *U1* is bent toward the ***F3b*** fracture, whereas the overlying layer *SCs1 (U2)* increases in thickness against it. The latter suggests that the deformation event that was called **Ev2** occurred

between the units *U1* and *U2*. As ***F3b*** extends above the horizon **Ev2**, it has thus been activated at least twice: during event **Ev2** and in a later event, **Ev1**. The ***F4*** system is composed of two major splays associated with the deformation zone induced by the dyke labeled ***Dy1***. ***F4b*** terminates at the horizon **Ev3**. ***F4a*** was activated after the event **Ev3** because it offsets this event horizon. The dyke ***Dy1*** below ***F4*** is mostly infilled with fine sands. This feature shows two branches at depth extending to the sandy layer *S4* in *U5*. This unit might be the source of the sand filling the dyke ***Dy1***. The south-western branch, ***Dy1b,*** is being cut by the northern one, ***Dy1a***, which suggests a two-phased deformation process. During the most recent phase of deformation, the ***Dy1a*** formed and the dyke extended to the top of the unit *U4*, strongly deforming the top layer *SCs5* in *U4*. It was later filled by gravels from the layer *Ch-G2* in *U3*. An event horizon is thus located at the *U3-U4* transition; it corresponds with the already identified **Ev4** horizon. During an earlier phase the northwestern splay ***Dy1b,*** which terminates within the convoluted layer *SC2* in *U4,* was activated. This phase may be associated with the event **Ev5**. The next dyke ***Dy2*** is rooted in the gravely unit *U3* and ends in the chaotic mélange. It shows two parallel walls deforming, on its NW side, the layers *S3, SCs4, S2* of the unit *U2* and a large widening above. This morphology suggests that dyking took place after the deposition of the layer *S2* in *U2* and that the free surface at the time of its activation was located near the top of *S2*. This level corresponds to the identified event horizon **Ev3**. The next sub vertical dyke ***Dy3*** extends from the trench bottom to the chaotic zone. It widens significantly downwards as it connects to the basal sandy unit *S3* in *U5*, which was probably the source bed. The vertical dyke ***Dy4*** apparently roots into *SCs6* and gradually widens upwards to end ~50 cm from the top of the outcrop. The silty clay unit *SCs1* in *U1* covers ***Dy4*** implying that a dyking event occurred just before the deposition of this layer. The corresponding event horizon is **Ev2**. The chaotic

deposit U_{Mel} against the SW wall of ***Dy4*** and the difference of deformation below and above the event horizon **Ev3** is evidence for an earlier deformation phase related to that event. The vertical dyke ***Dy5*** has similar geometry to ***Dy4***, but its NW wall reaches a higher level than ***Dy4***, suggesting a more recent dyking event, i.e. **Ev1**. The vertical dyke ***Dy6*** is larger, and roots below the outcrop bottom. It cuts across a strongly disturbed strata associated with an earlier dyking episode along the same structure. The chaotic strata U_{Mel} that outcrops on the SW side of ***Dy6*** would be associated with **Ev3,** because an undisturbed stratigraphy outcrops above this event horizon. Other dyke features are also identified more to the NE (see ***Dy7***).

The outcrop recorded the occurrence of five distinct episodes of deformation during which several dyking episodes occurred associated with the repeated deposition of the chaotic unit U_{Mel}. The latter is attested by the following facts: ***Dy3*** and ***Dy4*** crossed cut, at (H: 5.1m, V: 1.5m) in Fig. 8, the U_{Mel} unit deposited during an antecedent activation of the ***Dy4*** dyke in association with **Ev3**; ***Dy6*** and ***Dy7*** crossed cut at (H: 6.5m, V: 1m) the U_{Mel} unit deposited during an antecedent activation of the ***Dy6*** or ***Dy7*** dyke in association with **Ev5**; ***Dy5*** and ***Dy6*** crossed cut at (H: 6m, V: 1.25m) the U_{Mel} unit deposited during an antecedent activation of these dykes in association with **Ev3** and **Ev4** and at (H: 6m, V: 2m) the U_{Mel} unit probably deposited during **Ev2**. The episodes of deformation thus comprise fracturing, dyking and the concomitant deposition of a chaotic U_{Mel} unit**.** The presented event history holds because it relies on multiples and cross-cutting stratigraphic arguments: (1) multiple fracture and dyke terminations associated with a stratigraphy deformed during events, (2) sediments (e.g. U_{Mel}) deposited during events, (3) the occurrence of soft deformation (i.e **Ev5**). Our conclusions were also confirmed by sections adjacent the one logged. For example, the

Ev4 is evidenced on the same terrace riser, 20 m further to the SE of the studied section, by a thick soft deformation layer (see Appendice).

The U_{Mel} unit and the observed structural disturbances are intrinsically coupled and are interpreted to result from repeated seismically induced liquefaction. Earthquakes rupturing the nearby EAF or the Northwest Sivrice Fault have large magnitudes and generate seismic waves with high amplitude and strong duration that can induce the liquefaction of the saturated sediments present at depth in the Kürk Delta. The transformation of a solid to a liquid state of poorly compacted alluvial sediments induces a high pore-water pressure in the liquefied sediments that is then released by fracturing the overlying cap and by the upward venting of the liquefied material. In the studied section, only fractures and clastic dykes breaking the clay-rich cap are clearly visible. Along the same section, 15 m more to the North-east, a large bowl shape crater a typical of liquefaction feature was logged. The U_{Mel} unit would have been repeatedly emplaced during with the different liquefaction events. During the process, lacustrine sediments were ripped near the surface and along the wall of the dykes like for example at (H: 2.25m, V: 0) and at (H: 4.5m, V: 0.25m). Most of the mud clasts present in U_{Mel} are identical to the lacustrine sediments and are inferred to be derived from the strata cut by the dykes. The U_{Mel} unit is thus interpreted to represent the sediments expulsed from a liquefied source, mixed with the clay-rich sediments and gravels outcropping above, some being vented to the ground surface and others left behind in the vents/dykes. The dykes would result from the fracturing induced by the overpressure. The observed fractures and the dyke parallel walls suggest a development enhanced by tension cracks and by translational motion of the clay-rich blocks in between the dykes. These laterally moving landslides are called lateral spreading, and usually formed in association with

liquefaction processes. The source layer of the granular porous material that liquefied is not certain, but can be discussed. The geometry of ***Dy1*** and its sandy infill suggest that the sandy layer, *S4 (U5)*, partly visible at the outcrop bottom is a possible source. The sand in that unit is loose, fined grained, uniformly sized, and free of clay. It is this highly susceptible to liquefaction and displays no bedding or fabrics, which can be a consequence of its liquefaction. The U_{Mel} unit infilling the other dykes and present at the outcrop top could suggest a coarser and deeper source. This deeper gravelly source might correspond to unconsolidated alluvial sediments deposited during antecedent lowstands (Eriş, 2013). Liquefaction in gravelly deposits is considerably less common than in sandy deposits (e.g. Bezerraa et al., 2005) but occurred during modern-day M>6.5 earthquake (Yegian et al., 1994; Youd et al., 1985; Lunina and Gladkov, 2015). An other possibility is that most of gravels present in the U_{Mel} unit would have been derived from the gravel unit *U3* cut by the ***Dy2*** to ***Dy7*** dykes.

IMPACT OF LARGE EARTHQUAKE SHAKING ON THE SUBAQUEOUS DELTA

Morphological and structural imprints

The submarine delta plain had a classical morphology with a low dipping delta plain and a 20 m high front showing maximum dips of about 20° (Figs 7 and 9). This morphology was inherited from the large water level increase associated with the last glacial-interglacial transition (Eriş, 2013). Detailed examination of the delta shows complexities naturally related to the different deltaic bodies emplaced and then eroded (Fig. 7; Eriş, 2013) during large water level changes, but also due to seismic shaking. First, at around 9 to 10 m of water depth, the profiles showed 5° slopes related to the most recent deltaic complex, named Delta 3 (Eriş, 2013; Fig. 7). The upper part of Delta 3 contains disturbances breaking through the uppermost sedimentary infill (Fig. 7).

These structures are interpreted as extensional fractures and sediment extrusions related to an earthquake that induced a sudden increase of pore-fluid pressure, which triggered the liquefaction of coarse grained deposits, the hydraulic fracturation of the lacustrine mud drape and the lateral spreading. These seismically induced liquefaction features would be similar to the onland ones documented in the present paper. Similar features have indeed been related to seismically-induced liquefaction by Moernaut et al. (2009). Second, the sublacustrine delta plain systematically displays scarps and tension factures (Fig. 9) (Delta 2; Eriş, 2013; Fig. 7). These structural features are again interpreted as the result of earthquake ground motion and lateral spreading. Finally, the following large structural changes on the Kürk Delta might also have a seismic origin. The northern delta front is associated at depth with progradational structures that are lacking in its southern part (Fig. 9A). The southern delta front instead shows slide scarp features (Fig. 9B and C), and small mass wasting deposits are identified in front of the delta (Fig. 9B). This difference in morphology and structure can be interpreted as an effect of seismic shaking, which preferentially impacts the southern part of the delta. When an earthquake ruptures the NW Sivrice fault bounding the Kürk Delta or the main EAF segment located 2 km to the south, the southern part of the delta is more strongly shaken than its northern part, triggering larger destabilization events that impede sediment accumulation and delta propagation.

Sedimentological imprints

The most recent subaqueous fan sedimentation was studied using four sedimentary cores. Cores H003 and H002 sampled the nearshore environment in a water depth of about 5 m. They were located on the very low dipping surface that is continuous with the sub-aerial delta, at 150 m and 225 m respectively from the present shoreline (Fig. 2).

Core H005 sampled the sediments at a water depth of 20.5 m where the slope increased from 1° to 2° in relation with the Delta 2 (Eriş, 2013; Fig. 7). Core H006 was taken at a water depth of 57.6 m at the foot of the delta (Figs 2 and 7). At that location bottomset beds have a significant dip of 4-5 ° (Fig. 7). The cores were thus reflective of the sedimentation on the delta in the proximal (H002 and H003) and the distal (H005) environments, and of the lacustrine environments (H006) near the base of the delta front.

The cores are composed of homogeneous light brown clayey-silt with few dark brown coarser-grained silty-sand layers characterized in the X-Ray images by darker intervals (Figs 10 and 11). The clayey-silt deposits would be the background or continuous sedimentation due to from grain settling from the suspended sediment load while the sand-rich layers would be rapidly deposited layers or sedimentary events representing concentrated density flows coming from the Kürk River. Event layers have also a clay top settling from suspension. Different sedimentary event deposits were identified in the cores: the two main ones were labeled **E1** and **E2**, and the three minor ones **Ex, Ey** and **Ez**. In addition a significant color change occurring near the top of the cores was reported in the logs. The proposed core correlation was based on visible sedimentation changes, geophysical properties and sedimentary events (Figs 10 and 11). Because of their similar geophysical properties (see Fig. 11), event deposits **E1** and **E2** in all cores were inferred to be synchronous and correlative in the different cores. This inference was also supported by their relative position in the cores. These event deposits occurred at a deeper level in H003 and H002 than in H005 and H006 as expected because the sedimentation rate is larger in the near shore deltaic environment than in a more distal deltaic or lacustrine environment (Fig. 7).

Sedimentation rates were constrained using radionuclide dating. ^{137}Cs peaks related to the 1963 maximum of radioactive fallout and/or to the 1986 Tchernobyl event were identified. In H002 the first cesium peak appears 8.5 cm from the top and would be related to the Tchernobyl accident, whilst the second peak is located around 33 cm and must be linked to the 1963 peak (Fig. 12). Modelling ^{210}Pb exponential decay in conjunction with Cesium data suggested a mean sedimentation rate of 6 mm/yr at the H002 site. In H005 and H006, insignificant levels of Cs^{137} at respectively, 30 cm and at 20 cm depth implied a sedimentation rate lower than 6 mm/yr and 4 mm/yr respectively (Fig. 12). Higher cesium values at 3.5 cm in H005 and H006 associated with high ^{210}Pb activity could be related to the Tchernobyl event, and the peak at 14.5cm in H005 to the 1963 fallout peak, which implies a sedimentation rate of 3.5 mm/yr. Radionuclide data consistently indicated decreasing sedimentation rate from the proximal sites to the distal ones, and provided a framework to link changes in sedimentation with recent water fluctuations and seismic events. Radionuclide data indicated that events **E1** and **E2** took place 100 to 130 years ago, and that the three other events occurred in the last 60 years: event **Ez** around 1955, event **Ey** in the 70's and event **Ex** around 1986.

Analysis of continuous sedimentation comprising grain-size, mineralogy, organic matter and carbonate contents has shown that significant changes occurred (Figs. 10, 11, 13 and 14). Regarding grain-size, sedimentation is characterized at the different sites by about 95% silt-size particles (2-63 μm) and 2 to 1% sand-size particle at, respectively, proximal (H002, H003) and distal (H005, H006) sites (Fig. 10 and 11). Two major changes in grain size occur at the distal site H005 (Fig. 11). The most recent one takes place at 10.5 cm depth, after event deposit **Ey**, and is characterized by an increase in

sand-size particles. It also corresponds to a pronounced decrease in bulk density, probably linked to an increase in porosity. The other change in grain-size occurs at 26 cm depth after event deposit **Ez** and shows an increase in clay-size particles. Regarding mineralogy, sediments are composed of about 10 to 15% quartz, 25 to 35% clay, and 30% muscovite (Fig. 14). The cores show strong local variations regarding plagioclases, K-feldspar and aragonite. H003, the nearest shore core, has no aragonite suggesting an influence the Kürk River, which have a lower PH, alkalinity and chlorine content than the lake water (Şen and Topkaya, 1997; Şen and Gölbaşı 2008); H002 is enriched in plagioclases whereas H003 is enriched in K-feldspar**.** The cores recorded significant mineralogical changes. In H002, 30 cm below the top of the core and after event deposit **Ez**, plagioclases increase, and K-feldspar and quartz decrease. In H003, at 18.5 cm below core top and after event deposit **Ey**, K-feldspar and quartz increase, while plagioclase decrease. In H005, at depth shallower than 14 cm after event deposit **Ey**, plagioclases increase, and muscovite and clay decrease. Concerning organic and carbonate contents, the cores generally have shown opposite trends and similar changes. Carbonates increases toward the top of the cores, while organic matter decreases (Fig. 13). There is marked Ca-increase step after event deposit **Ey**.

Sedimentary events related to density flows are thicker and more strongly marked at the proximal sites H002 and H003 than at the distal site H005 (Figs 10 and 11). The lacustrine H006 site at the foot of the delta does not show additional events that could, for example, be related to a destabilization of the delta front. In all cores the two main closely spaced sedimentary event deposits, **E1** and **E2**, have magnetic susceptibility values at least 3 times greater than the average. The events have a similar imprint in all cores. The shallower event deposit **E1** has generally a higher magnetic susceptibility

than the **E2** event deposit. Both events have low carbonate and organic matter content (Fig. 13), coarse-grained content with a specific grain assemblage (Figs 10 and 11). The granulometric imprint is stronger at the proximal sites: In H002, event deposits **E1** and **E2** comprise, respectively, 16% and 9% of sand-size particles, although in H005 the intervals are only associated with an increase in sand-size particles of 1 to 2%. Scanning electron microscope data has shown that the event layers have a larger pore space than the hemipelagic sediments where clay particles strongly bound the coarser particles (Fig. 11C). As a result the density of these clastic layers are lower than the average at the H002 site (Fig 10A and 11A). **E1** and **E2** deposits are also associated with abrupt increases in plagioclase and/or K-feldspar (Fig. 14). These two high clastic content intervals with high magnetic susceptibility values were thus interpreted as resulting from a large allochtonous terrigenous input from the Kürk River.

The depositional processes associated with the two main sedimentary events, **E1** and **E2** were further characterized using high resolution microgranulometric measurements. Grain-size in combination with MS and density data showed that the upper event deposit **E1** in H002 consists of two distinct subunits (Fig. 10B). The basal interval is a 1.5 cm sand-rich unit with a sharp base and a normal grading; it corresponds to the high MS and low density interval. It is overlain by higher density interval enriched in clay-size particle. The lower event deposit **E2** is thicker and also shows two subunits: a 5 cm thick coarse base and a clay-enriched cap. The **E2** coarse basal unit is different from the **E1** one, as it shows four main low density sandy pulses. The coarsest pulse is the third one, and it corresponds to the highest MS values (Fig. 10A). **E1** and **E2** event deposits have different expressions in the other cores. The nearby proximal H003 core shows that event deposit **E1,** like event deposit **E2,** had several terrigenous pulses (Fig. 11). At

distal sites H005 and H006, the events are denser and show a gradual decrease in grain-size with a base including sandy particles and a clay enriched top; they are represented by a single MS peak corresponding to an increase in terrigenous particles. Finally, in all the cores, MS values were still higher than the background average value after the deposition of event deposit **E1**, suggesting a continuing terrigenous riverine contribution. The terrigenous inflow leading to the formation of these events was thus an order of magnitude higher than the one associated with the **Ex**, **Ey** and **Ez** events. Radionuclide measurements suggested that these events could be attributed to the 1874-1875 earthquake sequence. Historical records show the large imprint of the shocks on the lake and its catchment: landslide, liquefaction and a two-phase increase in water level (see section 2; Ambraseys, 1989). The possible processes responsible for these earthquake-related sedimentary deposits are further discussed in the next section.

The three other correlative clastic event deposits, **Ex**, **Ey** and **Ez** identified in the cores have the following characteristics. They are generally less coarse, thinner and strongly attenuated at the distal sites compared to **E1** and **E2** (Figs 10 and 11). They are often characterized by multiple clastic pulses particularly at the proximal sites where they also show a magnetic susceptibility imprint. Their trace in the sedimentation is often followed by a significant change in the long-term hemipelagic sedimentation. For example, the event deposit **Ey** is generally followed by a change in brightness in all cores and by a large increase in carbonates in H005 and H006 (Figs 10, 11 and 13). Event deposit **Ez** was followed by high carbonate content in all cores and by an increase in some terrigenous minerals in H003 and in H005 (Figs 13 and 14). These three events occurred in the last 60 years and would thus be related to a change in the lake limnology probably related to recent human-induced disturbances. The delta has been impacted by

two types of anthropic modifications. Firstly, a large water drop induced by hydroelectric pumping (Fig. 3) began after 1969 with a peak in 1973; since 1985, the lake level was stabilized and increased back slightly. Secondly, significant human-induced changes occurred on the subaerial part of the Kürk Delta since the 1950s. The town of Sivrice, located on the southern side of the fan, has grown significantly and the fan surface had started to be occupied and strongly modified. In particular, after the 1953 flooding, sediment dumping occurred on the delta, and between 1965 and 1975 the Sivrice population increased about 5 times (Fig. 5; Yiğit and Hayli, 1995). Growth was associated with the development of an industry on the Kürk Fan. Tile factories were established in 1966 and later in 1989 and 1991, producing several million tiles every year (Tonbul and Yiğit, 1995). They initially used raw materials from the Kürk Delta. A fertilizer factory was also opened in the 70's. Gravel extraction from the fan head occurred for construction purpose (Fig. 5). Finally the delta plain was fully cultivated. The following relationship between the sedimentary events and the anthropic disturbances is thus inferred. The oldest event **Ez** occurred around 1955 (Fig. 12); it would be linked to the 1953 flooding and to the following infilling and improvement of the infrastructure on the Kürk Delta. Events **Ey** and **Ex** occurred in the 70's and 80's. Event **Ey** was the most important one and was associated with large long-term changes in particular at the distal sites. It must have been linked to the abrupt anthropic water level drop. The large decrease in lake level could have had several consequences. In particular it would have triggered an increase in Total Inorganic Carbon by ion concentration, which could have been responsible for the observed increase in Carbonates (Fig. 13). Furthermore, a substantial reworking of sediments linked to the delta incision occurred. This would explain some of the sedimentological changes occurring after event deposit **Ey** like the general increase in magnetic susceptibility, and

in some terrigenous minerals. Finally the H003 site is located in close proximity to the clay extraction site of the large tile factory; the marked increase in quartz and K-feldspar after event deposit **Ey** in that core may be related to this exploitation. In conclusion a wealth of anthropic changes has impacted the sedimentation on the Kürk Delta, but it remains difficult to unambiguously link the events and the associated sedimentological changes with a single given cause.

DISCUSSION

Origin of lake level changes

Geophysical, historical and sedimentological data indicate the occurrence of large lake level changes in Lake Hazar characterized by the occurrence of two highstands, one during the 19th and the beginning 20th century and one before the 12th century. These water level changes may be linked to tectonic and/or climatic factors. Tectonic activity is a key factor because the outlet is affected by fault motion (Fig. 1; Garcia Moreno et al., 2010). Earthquake ruptures during highstand like in AD 1874-1875 would have a minimal impact on the water level that cannot rise above the 1253 m sill that forms the boundary with the Tigris catchment. The previous AD 1789 earthquake occurred during the 12th-18th Century lowstand and coincided with the lake level rise suggesting a tectonic triggering (Fig. 3). Climatic changes must have also impacted the lake water levels as Lake Hazar is during lowstand a closed lake which level depends on the precipitation:evaporation ratio. The 19th Century was an atypical climatic period characterized by very high water level in some Middle East lakes. In particular, the Dead Sea reached a particularly high anomalous level in the late 19th Century (Klein, 1961, 1986); this highstand was preceded by a lowstand, which had lasted since about

A.D. 1300 (Enzel et al., 2003). The water level variations of Lake Hazar seem to follow a trend similar to the Dead Sea, suggesting a limk with climatic changes.

Liquefaction and deformation features on the Kürk Delta and their use for paleoseismic purpose

The deformation episodes recorded in the onland outcrop of the delta (Fig. 8) have. most probably, been induced by repeated liquefaction and associated lateral spreading. Seismic reflection profiles also show on the subaqueous delta vertical fissures and deformation probably related to the same process. No other possible agents could have triggered the observed onland deformation. Deformation is not related to landsliding: the delta topography is flat and away from steep slopes. The upward flow of sediments cannot be related to artesian springs, again because of the lack of topographic relief. An additional criteria regarding our diagnostic is the spatial distribution pattern of the deformation (Obermeier, 1996). Our extensive study of the natural outcrops on the Kürk Delta show that lateral spreading and dyking is apparently restricted to the section we logged and its continuity to the south, but numerous soft deformation horizons are present and correlate laterally with the defined event horizons. In particular, our record of events can be correlated the seismically induced deformed horizons identified in Hempton and Dewey (1983), which can be mapped in a number of sedimentary outcrops investigated on the Kürk Delta (Figs 2 and 5). Five distinct horizons of earthquake induced soft sediment deformational structures were identified in 3 m high outcrops by Hempton and Dewey (1983). Their key stratigraphic section was located ~1 km to the SSE of our studied outcrop (Figs 2 and 5) and can be correlated to our section based on the common occurrence of the major lacustrine to fluvial transition related to the highstand to lowstand change that occurred in our section between *U3* and *U4* (Fig.

8). This transition took place before the 12^{th}-18^{th} century lowstand marked by the construction and occupation of the Armenian Monastery. A similar number of events were identified in both sections. The most recent deformed horizon identified by Hempton and Dewey (1983) occurred at the top of the stratigraphic column and correlates with the identified event horizon Ev1. A convoluted layer was also documented at the top of outcrops we prospected in some cases (Fig. 2): this deformed layer always occurred near or at the top of a thick silty clay lacustrine layer similar to the one logged at the top of the studied outcrop. The observed large extent of this event horizon supports the inferred seismic trigger. Similarly, the event horizon Ev4 located at or near the transition between the lacustrine-fluvial U4-U3 units had a broad extent, and correlates with the fourth event mapped in Hempton and Dewey (1983). For the other events not located at a marked stratigraphic discontinuity it was not possible to trace them extensively because of the lack of continuity of the outcrops, but the total number of events above or below the lowstand/highstand transition match the present record.

Earthquake induced liquefactions and lateral spreading have been widely documented in association with recent and historical earthquakes (e.g. Audemard and Santis, 1991; Kanibir et al., 2006; Yasuda et al., 2012; Rodriguez-Pascua et al., 2015; Bastin et al., 2015) and paleoliquefactions are usually interpreted as an evidence for seismic shaking (e.g. Obermeier, 1996). Episodic liquefactions at a given site have been used to infer a seismic history as for example in the Gulf of Corinth (Minos-Minopoulos et al., 2015), in the Himalaya (Kumar et al., 2016; Rajendran et al., 2016), or in the US intraplate interior (Obermeier et al., 1993; Tuttle and Barstow, 1996.). Indeed an important characteristic of the ground liquefaction is recurrence (Obermeier, 2009), and in the present case liquefaction use the same dykes for venting, a tendency that was noted in

some cases (Obermeier, 1996; Obermeier, 2009; Youd, 1984). A remaining important issue in our case regarding the use of the obtained liquefaction record for paleoseismic purpose is the systematic occurrence or not of this process during large earthquakes along the EAF. Liquefaction is strongly dependent on the presence of suitable saturated sediments at depth. Lake Hazar shows large water level changes probably associated with large variations in the water table that can change the liquefaction susceptibility. To check if the paleoseismic record obtained is complete, we compared the timing of the deformed horizons embedded in a stratigraphy linked to large water level changes to strong earthquakes occurring on the EAF. The most recent event horizon, **Ev1**, is located near the top of the erosional surface presently entrenched by the active stream, so **Ev1** predates the stream incision. This event horizon is observed near the top of the lacustrine unit *U1* that most likely was deposited during the 19th Century highstand, the event **Ev1** is thus attributed to the 1874-1875 earthquake sequence. The **Ev2** event horizon occurred just at the transition between the recent highstand unit *U1* and the lowstand unit *U2*. This suggests that the **Ev2** event would correspond to the 1789 earthquake that took place just before the large water level rise (Fig. 3). The link between the other liquefaction events **Ev3** and **Ev4** and historical earthquakes rupturing the EAF is more speculative. Events **Ev3** and **Ev4** took place during the deposition of the coarse-grained units *U2* and *U3* corresponding to the 12th-18th Century lowstand (Fig. 8). One of these events is recorded in a paleoseismic trench just to the east of Lake Hazar and would have occurred shortly after AD1420 just to the east of Lake Hazar (Çetin et al., 2003). The other might correspond with the AD 1285 historical earthquake, for which little information is available (Ambraseys, 2009). Finally, the **Ev5** event, which occurred during the antecedent highstand, would be the historical AD 995 earthquake that ruptured the EAF near Lake Hazar (Ambraseys and Jackson, 1998;

Ambraseys, 2009). The comparison thus suggests a systematic liquefaction process during large earthquakes, but radiocarbon dating of the section would be necessary for confirmation.

We conclude that the systematic liquefactions on the delta can used for paleoseismological purposes as an alternative to classical seismic trenching across the active fault trace. Several paleoseismic excavations were performed across the NW Sivrice Fault, where it had a clear expression and where recent alluvial sediments were present. A fault plane reaching the surface was identified in the trenches but the stratigraphy was so poor that it was no possible to constrain a sequence of events. On the opposite, the sediments of the Kürk delta display a large variety of facies and are a suitable paleoseismic recorder.

Origin of the earthquake related events on the subaqueous delta plain

The earthquake related **E1** and **E2** sedimentary events in all cores had the following characteristics (Figs 10, 11 and 14). They were coarse grained and composed of terrigenous materials characterized by high MS values. Their multiple distinct clastic pulses suggest that they result from multiple concentrated density flows not related to a unique paleoflood. In addition **E1** and **E2** are the largest event deposits that occurred in all the cores in the last 120 years, and their thicknesses did not decrease substantially across the delta. These rapidly deposited layers linked to density flows are different from the other commonly found seismites. Indeed, in lacustrine settings, seismites are generally related to turbidity flows induced by multiple slope gravitational failures (e.g., Schnellmann et al., 2002; Moernaut et al., 2007; Moernaut et al., 2014) or to the reworking of the lake slopes or floor (e.g. Moernaut et al., 2015; Hubert-Ferrari et al.,

2012). On a subaerial or near-shore delta, seismites are characterized by soft-sediment deformation induced by liquefaction and ground motion shearing (e.g. Heifetz et al., 2005; Agnon et al., 2006). Here the mechanism of deposition of the sedimentary events on the very low dipping plain near the H002 and H003 coring sites can not be directly linked either to slope failure, sediment resuspension nor to soft-sediment deformation.

The multiples density flows composing the events **E1** and **E2** that come from the Kürk River are interpreted to represent the mobilization and reworking of earthquake triggered landslides in the Kürk river catchment and of liquefaction products on the Kürk delta. Our interpretation is based on the following facts. Recent large magnitude earthquake in Taiwan (Dadson et al., 2004; Lin et al., 2008) and in China (Parker et al., 2011) have demonstrated that large shallow earthquakes trigger widespread, coseismic landslides that cause significant erosion (Keefer, 1994; Malamud et al., 2004). Regarding the 1874-1875 shocks along the EAF, they must have triggered significant mass failure along the steep slopes of the Kürk River Catchment (Fig. 1). Ambraseys (1989) showed that these earthquakes triggered large landslides, which caused the closing of mines in the area. The earthquake related landslides would become debris or mud flows during heavy rainfall events. Ultimately the remobilized sediments would be transported to the Kürk Delta as concentrated density flows. As a matter of fact, the 03/27/1875 and 05/03/1874 earthquakes occurred in the spring, a period during which the discharge of the Kürk River would be the greatest in response to snowmelt and rainfall (Günek and Yiğit, 1995; Sen and Topkaya, 1997). The multiple magnetic susceptibility peaks in H002 and H003 associated with events **E1** and **E2** would thus represent large magnitude density flows occurring at peak discharges of the Kürk River mostly during the spring after the 1875 and 1874 earthquakes. The coarse bases of the

events have thus not been deposited just after the earthquakes, but represent post-seismic sedimentary markers whose deposition on the delta took days or months depending on the river dynamics. The deposition process is thus intrinsically different from a classical coseismic turbidity flow related to a submarine mass wasting event triggered on the lake slopes at the time of the earthquake or to lake sediment remobilization (Moernaut et al., 2015): the basal layer of these deposits result from settling in the hours following the earthquakes. The distal cores H005 and H006 provide complementary information regarding the depositional pattern: the events are characterized by a basal high MS layer, darker and denser than the hemipelagic sedimentation but without visible laminations and large increase in sand-size particles. These characteristics suggest a strong and rapid dilution of the density flows that may even have evolved into an interflow. With the deposition of the coarsest particles nearshore, the relative increase of clay particles would damp the flow turbulence and enhance its cohesion. Its settling would thus involved both *en-masse* consolidation and incremental aggradation (e.g. Baas *et al*., 2011), a process responsible for the absence of distinct laminations and sharp grain-size contrasts. Hence the trace of these density flows in the deep basin would be very subtle. The proposed depositional scenario is presented in Fig. 15. Above the coarse base, the mud cap is interpreted to represent the classical settling of the muddy suspension cloud associated with any density flow; it would start during summer time when the river discharge was at its lowest point (Fig. 15). The fact that above the **E1** deposit magnetic susceptibilities values are still higher than the average background in the proximal or distal environments suggests that an increased terrigenous input from the Kürk River continues after the events (Figs 10, 11 and 15).

Post-earthquake flood-driven remobilization of liquefaction and landslides materials has been documented elsewhere in lacustrine environments. In particular, in a small lake in New Zealand located 3 km from the Alpine Fault, in which post-seismic sediment flux linked to earthquake shaking accounts for 27% of total sediment flux from the lake catchment (Howarth et al., 2012). In this mountainous context the postseismic increase in erosion last about five decades following large earthquakes. Hyperpycnal deposits were also observed above a co-seismic triggered turbidite in the Saguenay Fjord in Canada (St-Onge et al., 2012) or in the Lake Puyehue in Chili (Chapron et al., 2007). These deposits were interpreted to result from the rapid breaching and draining of natural dams created by earthquake-triggered landslides.

The case study of the Kürk Delta provides complementary information regarding this process. First, the thickness of event **E1** is comparable to **E2** ranging from 10.5 to 15 cm on the delta, and from 5 to 7 cm at the lacustrine site (Figs 10 and 11). The latter suggests that in steep mountainous terrains there is no limit in sedimentary supply from the catchment to the lake even if the time interval between the two earthquakes is very short. Second, a larger quantity of coarse grained material was provided during event E1, which shows coarser grain-size and larger MS values than **E2**. The first earthquake that triggered the deposition of **E2** must have considerably weakened the mountain slopes, the second lower magnitude earthquake that occurred shortly after is interpreted to have a larger sedimentary impact, still visible by the deposition of **E1**. So in the present case of two earthquakes close in time there are no obvious relation between earthquake magnitude and the thickness of the triggered sedimentary event. Third, the timing of the processes can be discussed because of the 11 months separating the **E2** event (1874/05/03) overlying the **E1** event (1875/03/27). The **E2** event contains multiple concentrated density flows that occurred mostly during the first year, probably

shortly after the event during spring. So the bulk of the event deposit accumulated in a relatively short period. Fourth the duration of the enhanced terrigenous supply attested by high MS values after the event **E1** at the proximal sites and the slightly coarser grain-size at the H005 distal site can be estimated. Based on hemipelagic sedimentation between the **E1** and **Ez** events, we inferred a post-seismic remobilization of ~30 years. The duration of the perturbation is similar to what was recorded in the New Zealand case (Howarth et al., 2012) even if the intensity of the long term reworking was not as high. In Taiwan, Hovius et al. (2011) estimate that following the Chi-Chi earthquake it took about 5 years for the concentration of suspended sediment in rivers to reach antecedent values. However Taiwan precipitation regime is very different from the East Anatolian one having a much higher rainfall and rain intensity (i.e typhon) that would be responsible for a more efficient reworking.

CONCLUSION

The Kürk Delta on the shores of the tectonic Hazar Lake has been repeatedly affected by lake-level change and by seismic shaking. Geophysical, remote sensing and sedimentological data confirms the following recent history of lake level fluctuations: (1) a recent (1970's) human induced lowstand; (2) a 19th Century highstand; (3) a 12th-18th Century lowstand during which an Armenian monastery was established; (4) a former highstand that formed a distinct deltaic complex (Delta 3). In addition to the lake level fluctuations that affected the delta tectonics also played a significant role. The delta is bound to the south by the NW Sivrice Fault and the Master Fault of the East Anatolian Fault System lies in close proximity. Seismic reflection profiles revealed recent scarps on both faults most probably related to the M>7 AD 1874 and M~6.5 AD 1875 earthquakes (Ambraseys, 1989). Repeated seismic shaking induced by large

magnitude earthquakes has let a wide diversity of imprints on the delta. First large-scale morphological and structural imprints were documented comprising tension cracks and sediment extrusion features probably related to lateral spreading, as well as minor landsliding along the delta front, preferentially near the active NW Sivrice Fault. Second, various sedimentological imprints were documented comprising (1) soft-sediment deformations already studied by Hempton and Dewey (1983); (2) large clastic dykes associated with brittle deformation that were interpreted as injection features induced by repeated liquefactions and associated lateral spreading; and (3) the occurrence of coarse grained terrigenous event deposits overlain by a clay cap on the subaqueous delta. The study of the latter deposits was based on the identification and characterization of the two seismites triggered by the AD 1874 and AD 1875 earthquakes in cores. Sedimentological analyses have shown that these event deposits are the largest in all the studied cores during the last 120 years, and that they result from several density flows and not from a unique paleoflood event. Our interpretation suggests that they result from multiple density flows induced by the reworking of terrestrial earthquake triggered landslides during spring-time peak flows of the Kürk River. The remobilization by flood events of most of the post-seismic materials deposited in the river catchment occurred rapidly in the first year after the earthquake, but an increased terrigenous signal persisted for about 30 years following the 1874 earthquake.

A paleoseismic history of large earthquakes impacting the Kürk Delta was also inferred based on the study of a deltaic sequence that outcropped following the 1970's lowstand. The section displays two fine-grained lacustrine units separated by a coarse grained delta plain unit, which would correspond to the 12^{th}-18^{th} Century lowstand. This section,

which would thus have been deposited over the last 1000 years, shows several dyke injection features associated with fracturing. These large structural disturbances were interpreted as being induced by repeated earthquake liquefactions and lateral spreading, Five event horizons (i.e. delta surface at the time of the earthquake) related to earthquake shaking were identified. The inferred seismic trigger is confirmed by (1) the correlation of all documented time horizons to soft-sediment deformation features documented in particular by Hempton et al. (1983); (2) the fact that the products of most recent dyking event outcrop at the top of the section and would have been triggered by the 1874-1875 sequence. Each liquefaction event was probably triggered by a near field large earthquake rupturing the EAF across or near the Hazar Lake. Recent water-level changes provide a temporal framework and implies a recurrence of about 250 years. The following paleoseismic history is thus recorded in the deltaic sequence: The most recent events occurred during the 19th lacustrine highstand and correspond to the 1874-1875 earthquake sequence; the second took place during the highstand-lowstand transition at the end of the 18th Century and is inferred to be the 1789 historical earthquake that ruptured the EAF near or across the lake (Ambraseys, 1989). The 5th occurred during the pre-12th century highstand, and matches the historical 995 earthquake rupturing the EAF near or across the lake (Ambraseys, 1989). Regarding the two events that occurred during the 12th-18th Century lowstand, their attribution to a given historical earthquake is more speculative, but a paleoseismic trench just to the east of the lake did document a rupture on the EAF shortly after AD1420 (Çetin et al., 2003) and a damaging historical earthquake occurred near Malatya in AD 1285 (Ambraseys, 2009).

The present study shows out that lacustrine deltas are particularly sensitive to earthquake shaking, which partly shapes their structure and stratigraphy. They should thus be considered as a potential paleoseismical target in addition to sites in the deep basins that are generally considered as natural seismometers (Howarth et al., 2014).

ACKNOWLEDGEMENT

This work was carried out in the frame of the Marie Curie Excellence Grant Project "Understanding the irregularity of seismic cycles: A case study in Turkey" (MEXT-CT-2005- 025617: Seismic Cycles) centered at the Seismology Section of the Royal Observatory of Belgium whom we would like to thank for their support. We are grateful for the assistance of Prof. Erhan Altunel of Osmangazi University for his assistance with logistics. The seismic lines were retrieved thanks to a fruitful collaboration with EMCOL (Eastern Mediterranean Centre for Oceanography and Limnology) and in particular Emre Damci. Logging in the field was done with the expertis of Jeff Fraser. We are indebted to X. Boes for his work during coring and on the cores: he acquired parts of the geophysical and geochronological data during his stay at the University of Rhode Island. Master student, Jean-Philippe Bouancheau also worked on the core H005 for his master thesis. PhD student Laura Lamair helped with the figures. The original manuscript was significantly improved thanks to the constructive reviews of Erhan Altunel, Katrin Monecke and the associate editor Manville Vern.

REFERENCES

Allen, J.R.L. (1982) Sedimentary structures, *vol. II. Developments in Sedimentology* **30B.** Elsevier, Amsterdam, pp. 663.

Ambraseys, N.N. (1989) Temporary seismic quiescence: SE Turkey. *Geophysical Journal* **96**, 311 – 331.

Ambraseys, N. and **Finkel, C**., (1995) The Seismicity of Turkey and Adjacent Areas 1500–1800, Eren, Istanbul.

Ambraseys, N.N. and **Melville, C.P.** (1995) Historical evidence of faulting in eastern Anatolia and northern Syria. *Annali di Geofisica* **38**, 337–343.

Ambraseys, N.N. and **Jackson, J.A.** (1998) Faulting associated with historical and recent earthquakes in the eastern Mediterranean region. *Geophysical Journal International* **133**, 390–406.

Ambraseys, N.N. (2009) Earthquakes in the Mediterranean and Middle East - A Multidisciplinary Study of Seismicity up to 1900, *Cambridge University Press*, pp. 968.

Agnon, A., Migowski, C. and **Marco, S. (**2006) Intraclast breccia layers in laminated sequences: recorders of paleo-earthquakes. In Enzel, Y., Agnon, A., and Stein, M., eds., New Frontiers in Dead Sea Paleoenvironmental Research, *Geological Society of America Special Paper* **401**, 195-214.

Anketell, J.M., Cegla, J. and Dzulynski, S. (1970). On the deformational structures in systems with reversed density gradients. *Ann. Geol. Soc. Pol.* **XL**, 3–30.

Audemard, A. and **De Santis, F. (**1991) Survey of liquefaction structures induced by recent moderate earthquakes. *Bulletin International Association of Engineering Geology* **44**, 5-16.

Aygün, Ç.Ö (2006) "Hazar Lake Sunken Settlement Elazıg, Turkey 2005 Survey Report", *FeRA(Frankfurter elektronische Rundschau zur Altertumskunde)* www.fera-journal.eu,
31-35.

Aygün, Ç.Ö. (2008) The Sunken Byzantine Settlement, 2005-2006 Underwater Survey at Hazar Lake Eastern Anatolia. 29. Uluslararası Kazı, Araştırma ve Arkeometri Sempozyumu, 25. Araştırma Sonuçları Toplantısı 3. Cilt, 159-170.

Bachrach, R., Nur, A. and **Agnon, A.** (2001) Liquefaction and dynamic poroelasticity in soft sediments. *Journal of Geophysical Research* **106**, doi: 10.1029/2000JB900474.

Baas, J.H., Best, J.L. and **Peakall, J.** (2001) Depositional processes, bedform development and hybrid bed formation in rapidly decelerated cohesive (mud-sand) sediment flows. *Sedimentology* **58,** 1953-1987.

Bastin, S.H., Quigley, M.C. and **Bassett, K.** (2015) Paleoliquefaction in Christchurch, New Zealand. *GSA Bulletin*, doi: 10.1130/B31174.1

Bezerraa, F.H.R., da Fonsecaa V.P., Vita-Finzi C., Lima-Filhoa, F.P., and **Saadic, A.** (2005) Liquefaction-induced structures in Quaternary alluvial gravels and gravelly sediments, NE Brazil. *Engineering Geology* **76** 191–208

Bowman, D., Korjenkov, A., and **Porat, N.,** (2004) Late-Pleistocene seismites from Lake Issyk-Kul, the Tien Shan range, Kyrghyzstan. *Sedimentary Geology* **163** 211–228

Bulut, F., Bohnhoff, M., Eken, T., Janssen, C., Kilic, T. and **Dresen, G.** (2012) The East Anatolian Fault Zone: Seismotectonic setting and spatiotemporal characteristics of seismicity based on precise earthquake locations. *Journal of Geophysical Research* **117**, B07304, 10.1029/2011JB008966

Çetin, H., Guneyli, H. and **Mayer, L.** (2003) Paleoseismology of the Palu-Lake Hazar segment of the East Anatolian Fault Zone, Turkey. *Tectonophysics* **374**, 163 – 197.

Chapron, E., Juvigné, E., Mulsow, S., Ariztegui, D., Magand, O., Bertrand, S., Pino, M. and **Chapron, O.** (2007) Recent clastic sedimentation processes in Lake Puyehue (Chilean Lake District, 40.5°S). *Sedimentary Geology* **201**, 365–385, doi:10.1016/j.sedgeo.2007 .07.006.

Dadson, S.J., Hovius, N., Chen, H., Dade, W.B., Lin, J.-C., Hsu, H.-L., Lin, C.-W., Horng, M.-J., Chen, T.-C., Milliman, J. and **Stark C.P.** (2004) Earthquake-triggered increase in sediment delivery from an active mountain belt. *Geology* **32**, 733-736.

Duman, T.Y. and **Emre, O.** (2013) The East Anatolian Fault: geometry, segmentation and jog characteristics, *Geological Society, London, Special Publications* **372**, doi 10.1144/SP372.14

Dunne, L.A. and **Hempton, M.R.** (1984) Deltaic sedimentation in the Lake Hazar pull-apart basin, south-eastern Turkey. *Sedimentology* **31**, 401 – 412

El-Isa, Z.H. and **Mustafa, H.** (1986) Earthquake deformations in the Lisan deposits and seismotectonic implications, *Geophys. J. R. Astron. Soc.* **86**, 413–424.

Enzel, Y., Kadan, G. and **Eyal, Y.** (2000). Holocene earthquakes inferred from a fan-delta sequence in the Dead Sea graben. *Quat. Res.* **53** (1), 34–48.

Enzel, Y., Ken-Tor, R., Sharon, D., Stein, M., Gvirtzman, H. and **Dayan, U.** (2003). Dead Sea lake level variations and Holocene climates in the Near East: implications to historical responses and modern water resources. *Quaternary Research* **60**, 263–273.

Ettensohn, F.R., Rast, N. and **Brett, C.E.** (2002). Ancient Seismites. *Geological Society of America*, p. 190.

Eriş, K.K. (2013), Late PleistoceneeHolocene sedimentary records of climate and lake-level changes in Lake Hazar, eastern Anatolia, Turkey. *Quaternary International* **302**, 123-134

Garcia Moreno, D., Hubert-Ferrari, A., Moernaut, J., Fraser, J., Boes, X, Van Daele, M., De Batist, M., Damci, E. and **Cagatay, N.** (2010) Structure and evolution of Lake Hazar pull-apart Basin along the East Anatolian Fault. *Basin Research* **23**,191-207, doi: 10.1111/j.1365-2117.2010.00476.

Goldberg, E.D. (1963). Geochronology with ^{210}Pb. [In:] *Radioactive Dating, International Atomic*

Energy Agency, Vienna, 121-130.

Guidoboni, E., Comastri, A. and **Traina, G.** (1994) Catalogue of Ancient Earthquakes in the Mediterranean Area up to the 10th Century, *Istituto Naz. di Geofisica*, Rome. pp.504.

Günek, H. and **Yiğit, A.** (1995) Hazar Gölü Havzasının Hidrografik Özellikleri. *1.Hazar Gölü ve Çevresi Sempozyumu*, **91–103**, Sivrice-Elazığ.

Heifetz, E., Agnon, A. and **Marco, S.** (2005) Soft sediment deformation by Kelvin Helmholtz Instability: A case from Dead Sea earthquakes. *Earth and Planetary Science Letters* **236,** 497–504.

Hempton, M.R. and **Dewey, J.F.** (1983) Earthquake-induced deformational structures in young lacustrine sediments, East Anatolian Fault, southeast Turkey. *Tectonophysics* **98**, 7 – 14.

Hempton, M.R., Dunne, L.A. and **Dewey, J.F.** (1983) Sedimentation in an active strike-slip basin, southeastern Turkey. *The Journal of Geology* **91**, 401-412.

Hovius, N., Meunier, P., Lin, C., Chen, H., Chen, Y., Dadson, S., Ming-Jame, H. and **Lines M.** (2011) Prolonged seismically induced erosion and the mass balance of a large earthquake. Earth Planet Sci Lett. doi:10.1016/j.epsl.2011.02.005

Howarth, J.D., Sean J., Fitzsimons, S.J., Richard, J., Norris, R.J. and **Jacobsen, G.E.** (2012) Lake sediments record cycles of sediment flux driven by large earthquakes on the Alpine fault, New Zealand. *Geology* **40**. 1091-1094 doi: 10.1130/G33486.1

Howarth, J.D., Fitzsimons, S. J., Norris, R.J. and **Jacobsen, G. E.** (2014) Lake Sediments record high intensity shaking that provides insight into the location and rupture length of large earthquakes on the Alpine Fault, New Zealand. *Earth and Planetary Science Letters* **403**, 340-351.

Hubert-Ferrari A., Boes, X., Fraser, J., Avsar, U., Vanneste, K., Cagatay, N., Altunel, E., de Batist, M. and **Fagel, N.** (2007) Understanding the irregularity of Seismic cycles: A Case study in Turkey-A Marie Curie Excellence Team Project. European Geosciences Union Meeting, *Geophysical Research Abstract* **9**, 06720.

Hubert-Ferrari, A., King, G., Van Der Woerd, J., Villa, I., Altunel, E. and **Armijo, R.** (2008) Long-Term Evolution of the North Anatolian Fault: New Constraints from its Eastern Termination. In 'Geodynamics of Collision and Collapse at the Africa-Arabia-Eurasia Subduction Zone'. *Geological Society, Special publication*. Editors: Douwe van Hinsbergen, Mike Edwards, Rob Govers.

Hubert-Ferrari, A., Avsar, U., El Ouahabi, M., Lepoint, G., Martinez, P. and **Fagel, N.** (2012) Paleoseismic record obtained by coring a sag-pond along the North Anatolian Fault (Turkey). *Annals of Geophysics* **55**, 929–953. http://dx.doi.org/10.4401/ag-5460.

Kanibir, A., Ulusay, R. and **Aydan, O.** (2006) Assessment of liquefaction and lateral spreading on the shore of Lake Sapanca during the Kocaeli (Turkey) earthquake, *Engineering Geology* **83**, 307–331.

Keefer, D.K. (1994) The importance of earthquake-induced landslides to long-term slope erosion and slope-failure hazards in seismically active regions. *Geomorphology* **10**, 265–284.

Ken-Tor, R., Agnon, A., Enzel, Y., Marco, S., Negendank, J.F.W. and **Stein, M.** (2001) High-resolution geological record of historic earthquakes in the Dead Sea basin. *Journal of Geophysical Research* **106**, 2221–2234, doi: 10.1029/2000JB900313.

Klein, C. (1961). On Fluctuations of the Level of the Dead Sea Since the Beginning of the 19th Century, *Hydrological Paper* **7**. Israel Hydrological Service, Jerusalem.

Klein, C. (1986). Fluctuations of the Level of the Dead Sea and Climatic Fluctuations during Historical Times. *Ph.D. dissertation, Hebrew University, Jerusalem*. [In Hebrew with English abstract].

Kumar, D., Reddy, D.V. and **Pandey, A.K.** (2016) Paleoseismic investigations in the Kopili Fault Zone of North East India: Evidences from liquefaction chronology, *Tectonophysics* **674**, 65–75.

Lemcke, G. and **Sturm, M. (**1997). $\delta^{18}O$ and trace element measurements as proxy for the reconstruction of climate changes at Lake Van (Turkey): Preliminary results. *In* Dalfes, H.N., Kukla, G., and Weiss, H. (Eds.), *Third Millennium BC Climate Change and Old World Collapse*. *NATO ASI Series I, Global Environmental Change **49**:* Berlin (Springer), 653–78.

Lin, G.-W., Chen, H., Hovius, N. Horng, M.J., Dadson, S., Meunier, P. and **Lines, M.**, (2008) Effects of earthquake and cyclone sequencing on landsliding and fluvial sediment transfer in a mountain catchment. *Earth Surf. Process. Landforms* **33**, 1354–1373 DOI: 10.1002/esp.1716

Lunina, O.V. and **Gladkov, A.S.** (2015) Seismically induced clastic dikes as a potential approach for the estimation of the lower-bound magnitude/intensity of paleoearthquakes, *Engineering Geology* **195,** 206–213.

Machlus, M., Enzel, Y., Goldstein, S.L., Marco, S. and **Stein, M. (**2000) Reconstructing low levels of Lake Lisan by correlating fan-delta and lacustrine deposits. *Quaternary International* **73/74**, 137-144.

Malamud, B.D., Turcotte, D. L., Guzzetti, F. and **Reichenbach, P.** (2004) Landslide inventories and their statistical properties. *Earth Surf. Processes Landforms* **29**, 687–711.

McCalpin J.P. (2009) Paleoseismology, Academic Press, 629 pages.

Minos-Minopoulos, D., Pavlopoulos, K., Apostolopoulos, G., Lekkas, E. and **Dominey-Howes, D.** (2015) Liquefaction features at an archaeological site: Investigations of past earthquake events at the Early Christian Basilica, Ancient Lechaion Harbour, Corinth, Greece, **Tectonophysics** 658, 74–90.

Moernaut, J., De Batist, M., Charlet, F., Heirman, K., Chapron, E., Pino, M., Brümmer, R. and **Urrutia, R.** (2007) Giant earthquakes in South-Central Chile revealed by Holocene mass-wasting events

in Lake Puyehue, *Sedimentary Geology* **195**, 239–256.

Moernaut, J., De Batist, M., Heirman, K., Van Daele, M. , Pino, M., Brümmer, R. and **Urrutia, R.** (2009) Fluidization of buried mass-wasting deposits in lake sediments and its relevance for paleoseismology: Results from a reflection seismic study of lakes Villarrica and Calafquén (South-Central Chile). *Sedimentary Geology* **213**, 121–135.

Moernaut, J., Daele, M. V., Heirman, K., Fontijn, K., Strasser, M., Pino, M., Urrutia, R. and **De Batist, M.** (2014) Lacustrine turbidites as a tool for quantitative earthquake reconstruction: New evidence for a variable rupture mode in south central Chile, *J. Geophys. Res. Solid Earth* **119**, 1607–1633, doi:10.1002/ 2013JB010738.

Moernaut, J., Daele, M. V., Clare, M.A., Heirman, K., Viel M., Cardenas, J., Kilian R., Ladrón de Guevara, B., Pino, M., Urrutia, R. and **De Batist, M.** (2014) Lacustrine turbidites produced by surficial slope sediment remobilization: A mechanism for continuous and sensitive turbidite paleoseismic records, Marine Geology, accepted.

Montenat, C., Barrier, P., Ott d'Evestou, P. and **Hibsch, C.** (2007) Seismites: an attempt at critical analysis and classification. *Sedimentary geology* **196**, 5-30.

Obermeier, S.F., Martin, J.R., Frankel, A.D., Youd, T.L., Munson, P.J., Munson, C.A. and **Pond, E.C.** (1993) Liquefaction Evidence for One or More Strong Holocene Earthquakes in the Wabash Valley of Southern Indiana and Illinois, Which a Preliminary Estimate of Magnitude. **United States Geological Survey, Professional Paper** 1536.

Obermeier, S.F. (1996) Use of liquefaction-induced features for paleoseismic analysis - An overview of how seismic liquefaction features can be distinguished from other features and how their regional distribution and properties of source sediment can be used to infer the location and strength of Holocene paleo-earthquakes, US Geological Survey, Reston, VA 20192, USA, *Engineering Geology* **44** (1). DOI: 10.1016/S0013-7952(96)00040-3.

Obermeier, S.F. (2009) Using Liquefaction-induced and other soft-sediment features for paleoseismic analysis. *In*: McCaplin, J. (Ed.), *Paleoseismology*. *International Geophysics* **95**. http://dx.doi.org/10.1016/S0074-6142(09)95007-0.

Parker, R.N., Densmore, A.L., Nicholas, J. R., de Michele, M., Li, Y., Huang, R., Whadcoat, S. and **Petley, D.N. (**2011) Mass wasting triggered by the 2008 Wenchuan earthquake is greater than orogenic growth. *Nature Geoscience* **4**, 449–452 doi:10.1038/ngeo1154.

Rajendran, C. P., John, B., Rajendran, K. and **Sanwal, J.** (2016) Liquefaction record of the great 1934 earthquake predecessors from the north Bihar alluvial plains of India, *Journal of Seismology*, 1-13.

Reilinger, R., McClusky, S., Vernant, P., Lawrence, S., Ergintav, S., Cakmak, R., Ozener, H., Kadirov, F., Guliev, I., Stepanyan, R., Nadariya, M., Hahubia, G., Mahmoud, S., Sakr, K., ArRajehi, A., Paradissis, D., Al-Aydrus, A., Prilepin, M., Guseva, T., Evren, E., Dmitrotsa, A., Filikov, S.V., Gomez, F., Al-Ghazzi, R. and **Karam, G. (**2006) GPS constraints on continental deformation in the Africa-Arabia-Eurasia continental collision zone and implications for the dynamics of plate interactions. *Journal of Geophysical Research*, **111**, B05411, doi: 10.1029/2005JB004051.

Rodriguez Pascua, M. A., Calvo, J.P., De Vicente, G. and **Gomez-Gras (**2000) Soft-sediment deformation structures interpreted as seismites in lacustrine sediments of the Prebetic Zone, SE Spain, and their potential use as indicators of earthquake magnitudes during the late Miocene. *Sed. Geol.* **135**, 117–135.

Rodriguez-Pascua, M.A., Silva, P.G., Pérez-López, R., Giner-Robles, J.L., Martín-González, F. and **Del Moral, B.** (2015) Polygenetic sand volcanoes: on the features of liquefaction pro- cesses generated by a single event (2012 Emilia Romagna 5.9 Mw earthquake, Italy. *Quaternary International* **357**, 329–335.

Şaroğlu, F., Emre, Ö. and **Küçu** (1992) The East Anatolian Fault zone of Turkey. *Annales Tectonicae*, **99** – 125 (Special Issue-Supplement to Volume **VI**).

Schnellmann, M., Anselmetti, F.S., Giardini, D., McKenzie, J.A. and **Ward, S.N.** (2002) Prehistoric earthquake history revealed by lacustrine slump deposits. *Geology* **30**, 1131–1134, doi:10.1130/0091-7613.

Seilacher, A. (1969) Fault-graded beds interpreted as seismites. *Sedimentology* **13**, 155–159.

Şen, B. and **Topkaya, B.** (1997) Lake Hazar (Elazig) and its characteristics, in Conservation and Management of Lakes, Reservoirs and wetlands in Turkey. *International Lake Environment committee, Japa*n, 163-188.

Şen, B., Koçer, M.A.T., Canpolat, Ö., Alp, M.T., Çetin, A.K., Türkgülü İ. and **Sönmez, F.** (2007) Pollution and siltation effects of the running waters on Lake Hazar and restoration practice to minimize these threats. *International Congress on River Basin Management* **1**, 308–318.

Şen, B. and **Gölbaşı S.** (2008) Hazar Gölü'ne Dökülen Kürk Çayı'nın Bazı Fiziksel ve Kimyasal Ozellikleri, *E.U. Journal of Fisheries & Aquatic Sciences* **25**, 353–358

Şengör, A.M.C. and **Yılmaz, Y.** (1981) Tethyan evolution of Turkey: a plate tectonic approach. *Tectonophysics* **75**, 181–241.

Stine, S. (1990). Late Holocene fluctuations of Mono Lake, eastern California. *Paleogeography Paleoclimatology Paleoecology* **78**, 333-381.

St-Onge, G., Chapron, E., Mulsow, S., Salas, M., Viel, M., M Debret, A Foucher, Mulder T., Winiarski T., Desmet M., Costa P JM, Ghaleb B., Jaouen A. and **Locat J.** (2012) Comparison of earthquake-triggered turbidites from the Saguenay (Eastern Canada) and Reloncavi (Chilean margin) Fjords: implications for paleoseismicity and sedimentology. *Sedimentary Geology* **243-244**, 89-107.

Tonbul, S. and **Yiğit, A.** (1995) Pleyistosen'den Günümüze Hazar Gölü'ndeki Seviye Değişmeleri, Çevresel Etkileri ve Hatunköy Kapması, *1. Hazar Gölü ve Çevresi Sempozyumu* **41–69**, Sivrice-Elazığ.

Tuttle, M.P. and **Barstow, N. (**1996) Liquefaction-related ground failure: a case study in the New Madrid seismic zone, Central United States. *Bulletin of the Seismological Society of America* **86**, 636-645.

Tuttle, M.P. (2001) The use of liquefaction features in paleoseismology: Lessons learned in the New Madrid seismic zone, central United States. *Journal of Seismology* **5**, 361-380.

Wetzler, N., Marco, S. and **Heifetz, E. (**2010) Quantitative analysis of seismogenic shear-induced turbulence in lake sediments. *Geology* **8**, 303 –306.

Wick, L., Lemcke, G. and **Sturm, M. (**2003) Evidence of Late Glacial and Holocene climatic change and human impact in Eastern Anatolia: high-resolution pollen, charcoal, isotopic and geochemical records from the laminated sediments of Lake Van, Turkey. *Holocene* **13 (5),** 665–675.

Yasuda, S., Harada, K., Ishikawa, K. and **Kanemaru, Y.** (2012) Characteristics of lique- faction in Tokyo bay area by the Great East Japan earthquake. *Soils and Foundations* **52**, 793-810.

Yegian, M.K., Ghahraman, V.G., Members, A.S.C.E. and **Harutiunyan, R.N.** (1994) Liquefaction and embankment failure case histories, 1988 Armenian Earthquake. *Journal of Geotechnical Engineering* **120**, 581–596.

Yiğit, A. (1995) Hazar Gölü Suları Altında Kalan Gölcük Köyü Hakkında Bir Tarihi Coğrafya Araştırması,1. *Hazar Gölü ve Çevresi Sempozyumu,* 185–188, Sivrice-Elazığ.

Yiğit, A. and **Hayli, S. (**1995) Hazar Gölü ve Behrimaz Havzalarında Kır Yerleşmelerinin Coğrafi Özellikleri,1. *Hazar Gölü ve Çevresi Sempozyumu*, 203–218, Sivrice-Elazığ.

Yönlü, Ö, Altunel, E., Karabacak V. and **Akyüz, H.S. (**2013) Evolution of the Gölbaşı basin and its implications for the long-term offset on the East Anatolian Fault Zone, Turkey. *Journal of Geodynamics*

65, 272–281

Youd, T.L. (1984) Recurrence of liquefaction at the same site. *Proceedings of the Eighth World Conference on Earthquake Engineering*, Earthquake Engineering Research Institute, San Francisco, Calif. **3**, 231–238

Youd, T.L., Harp, E.L., Keefer, D.K. and **Wilson, R.C.** (1985) The Borah Peak, Idaho earthquake of Oct. 28, 1983—liquefaction. *Earthquake Spectra* **2**, 71 – 89.

FIGURE LEGENDS

Figure 1. Lake Hazar and the associated Kürk Delta crossed by the East Anatolian Fault (EAF) and its Master Fault (MF). Secondary faults comprise the Northern Fault (NF), the Southern Gezin (S Gezin F) and the North-western Sivrice Faults (NW Sivrice F) The white triangle indicates the sunken Armenian settlement and the Kilise Island (Gölcük Adasi; Yiğit, 1995; Aygün, 2006) on the southern shore. Lower right inset shows the tectonic context: the extrusion of the Anatolian Plate accommodated in particular by the EAF and the North Anatolian Fault (NAF) as evidenced by geodetic data (Reilinger et al., 2006). Lake Hazar (LH) is indicated by a star. The upper left inset is a slope map of the Kürk catchment.

Figure 2. A: Map of the Kürk Delta at the WSW extremity of Lake Hazar. The submarine delta front was mapped based on seismic data (white dash lines for its top and bottom). The Delta is bounded to the South by the North-western Sivrice Fault and by small secondary deltas. Thin black plain and dash lines are respectively selected sparker and Innomar seismic-reflection profiles from Figs 4, 7 and 9. The studied delta outcrop and sedimentary cores are marked as well as additional prospected outcrops and

stratigraphic profiles studied by Hempton et al. (1983). MF: Master Fault of the East Anatolian Fault System. The mosaics of the georeferenced side scan sonar data in the sunken settlement area around the Kilise Island are outlined. **B.** Photo of the Kürk Delta and the Sivrice City. Viewpoint indicated in A.

Figure 3. Historical lake level changes of Lake Hazar modified from Tonbul and Yiğit (1995) with levels inferred from historical data (grey) and levels monitored since 1957 by the state agency (black) responsible for the utilization of water resources in Turkey (i.e. DSI). The figure also indicates the two known overflows of the Tigris River in 1911 and 1953, which occurred when the lake level reached 1253 m. Historical references from Tonbul and Yiğit (1995) are [1] Dupré, A. 1819. Voyage en Perse, fait dans les années 1807, 1808 et 1809 en traversant l'Anatolie et Mésopotamie. cilt 1, Paris; [2] Ritter, C. 1843. Die Erdkunde von Asien cilt 10, s.104-107, Berlin; [3] Hommaire de Hell, X. 1854. Voyage en Turquie et en Perse, exécuté en 1846, 1847 et 1848. cilt I. s.433, Paris; [4] Tozer, H.F. 1881. Turkish Armenia and Eastern Asia Minor. London. 238-246; [5] Huntington, E. 1902. The valley of upper Euphrates River and its people. Bull. of the Amer. Geogr. soc. 34, 388–389, New York.

Figure 4. Seismic reflection profiles showing recent surface ruptures along the NW Sivrice Fault in **A** at the foot of the Kürk sublacustrine Delta (profile p2) and in **B** along the EAF (profile p3). Profiles location is indicated in Fig. 2. Ruptures showing a recent vertical apparent scarp greater than 1 m and associated deformation are attributed to the 1874-1875 earthquake sequence.

Figure 5. Recent changes on the Kürk subaerial Delta. Left: Corona image taken in Dec. 1960 with topographic (thin dash black contour lines) and geographic (road, swamps) information from imagery taken in 1952 and 1955; Right: Google Earth image taken in 2010. The comparison highlights the recent lake level drop, channeling of the river into two branches, expansion of Sivrice Town and the development of the road network, industrial sites and agricultural fields on the fan. The study outcrop was located along the lake shore in the 1950's.

Figure 6. The sunked Armenian settlement and the lowstand surface.

A. Map of settlement imaged by side-scan sonar on the right (see location in Figs 1 and 2) and on the left selected side-scan images of part of the monastery and its two protective walls. Location of the seismic line in B is indicated. **B.** High frequency seismic reflection profile across the second protective wall. Right inset present the low frequency profile. Data were taken at the same time as the side-scan and show that the fortifications are presently under 10 m water depth. The Unconformity labeled U corresponding to the 12^{th}-18^{th} Century lowstand and the overlying 19^{th}-20^{th} Century muddrap labeled A are identified.

Figure 7. The Kürk Delta and the 12^{th}-18^{th} Century lowstand surface. The submarine depositional system is composed of three main deltaic complexes identified in Eriş (2013): a large slope break in A. at the delta front associated with the oldest complex, Delta 1, and a delta plain with a small change in slope in B. associated with the deltaic complex 2 (Delta 2). Location of the seismic profile p1 is indicated in Fig. 2. Inset C shows the youngest and shallowest deltaic deposit, Delta 3, whose toposets were eroded, probably during the 12^{th}-18^{th} Century lowstand. Potential liquefaction features

similar to the ones documented onland are imaged. Inset D shows the lowstand unconformity U, the lowstand facies B that has a high reflective discontinuous pattern and the ~ 1 m thick transgressive mud drape A on top, deposited during the 19^{th}-20^{th} Century highstand.

Figure 8. Studied section through the onland delta plain. **A.** Photo with on the right and left enlargements showing liquefaction dykes and fractures. **B.** Outcrop log showing four sedimentary units emplaced during periods characterized by different lake levels. In particular the top clayed unit *U1* was deposited during a high stand, and the coarse grained units *U3 and U2* characterized by the occurrence of channels during a lowstand. The stratigraphy is disrupted by dyking and the associated brittle deformation related to repeated earthquake liquefaction characterized by the concomitant deposition of the chaotic unit, U_{Mel} and by lateral spreading. Five different event horizons are identified.

Figure 9. Seismic profiles highlighting the Kürk Delta structure with scarps, tension factures and small-scale mass-wasting potentially related to lateral spreading and ultimately to seismic shaking. The changing structure of the delta with in **A** a prograding structure and in **B** and **C** a destabilized slope indicates that the southern part of the delta is more strongly destabilized by earthquake shaking. Location of the seismic profiles is indicated in Figure 2.

Figure 10. Sedimentary core H003. **A.** Photo, radiography, log, brightness and geophysical measurements (Magnetic susceptibility, density, electrical resistivity). Two main sedimentary event deposits **E1** and **E2** as well as secondary event deposits (**Ex,**

Ey, Ez) are identified. Label 2 indicates location of MEB sample 2 in Figure 10. **B.** Sand, silt and clay fraction of the sedimentary event deposits **E1** and **E2**.

Figure 11. Sedimentary cores H002, H005, H006. **A.** Photo, radiography, log, brightness and geophysical measurements (Magnetic susceptibility, density, electrical resistivity). Label 1, 3, 4, 5 indicates location of MEB samples in C. **B.** Sand, silt and clay fraction of the core H005 showing large changes in the settling parameters associated with recent secondary sedimentary events. **C.** MEB images of the sedimentary event deposits **E1** (2 in H002 see Fig. 8, 3 in H005, 5 in H006) and **E2** (4 in H005), and of the background sedimentation (1). Location of samples in A and in Figure 9.

Figure 12. ^{210}Pb and ^{137} Cs radionuclide measurements in cores H002, H005, H006. Core H002 sampling the proximal deltaic site shows ^{137} Cs peaks probably related to the 1986 Tchernonyl event and to the 1963 maximum fallout; ^{210}Pb and ^{137}Cs data imply a sedimentation rate of 6 mm/yr. Core H005 at distal deltaic site and core H006 at the delta foot have lower sedimentation; 1963 ^{137}Cs peak at 14.5 cm implies a sedimentation rate of 3 mm/yr.

Figure 13. Cores H002, H003, H005 and H006 and LOI data (% carbon in black and %carbonate in grey). Organic and carbonates contents show similar changes in the different cores and opposites trends with lower organic matter and higher carbonate content at the top of the core, which is related to the recent decrease in water level (Fig. 3).

Figure 14. Mineralogy of cores H002, H003 and H005. All cores show large changes near the top corresponding to anthropogenic perturbations of the sedimentation on the sub-aerial delta.

Figure 15. Schematic representation of the deposition of the sedimentary event deposits on the delta at proximal and distal sites. In top diagram, deposition of the bulk of the sedimentary events by density flows resulting from peak flows of the Kürk River reworking landslides in its catchment. Dilution increases from the proximal to the distal sites, which leads to a decrease in coarse sediment content and in turbulence because of the higher clay content increasing the flow cohesion. Deposition is thus dissimilar at proximal and distal sites as illustrated in the columnar sections. In middle diagram, deposition of the clay cap above the coarsest event basal layers due to settling of the muddy suspension cloud associated with density flows during low river discharge. In bottom diagram, deposition of hemipelagic sedimentation with a higher magnetic susceptibility rate due to slightly higher sediments terrigeneous loose sediments.

Figure 1.

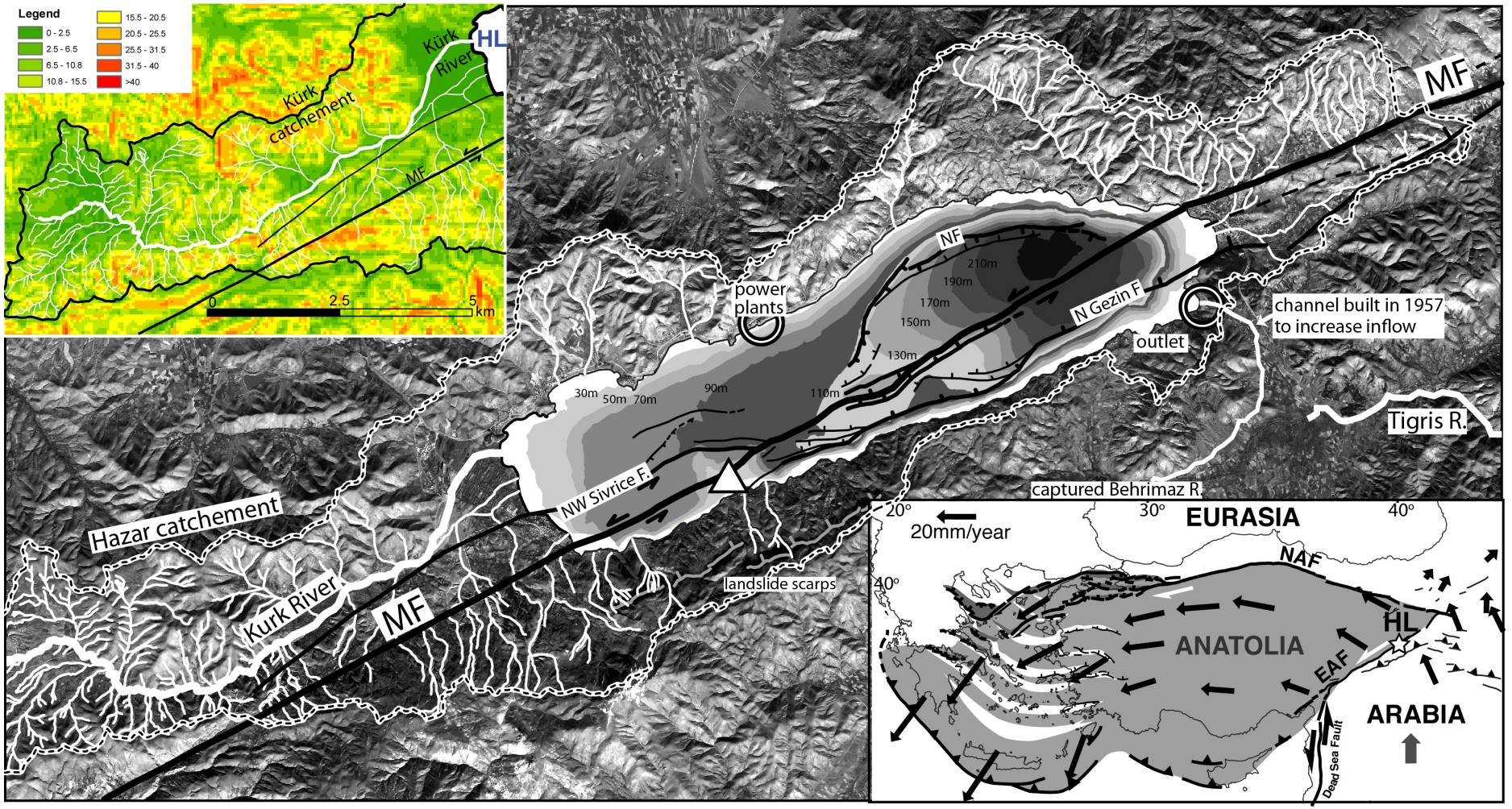
Legend
0 - 2.5
2.5 - 6.5
6.5 - 10.8
10.8 - 15.5
15.5 - 20.5
20.5 - 25.5
25.5 - 31.5
31.5 - 40
>40
Kürk River
HL
Kürk catchement
MF
0
2.5
5
km
NF
210m
190m
170m
150m
130m
110m
90m
30m
50m
70m
power plants
N Gezin F
outlet
channel built in 1957
to increase inflow
Tigris R.
captured Behrimaz R.
NW Sivrice F.
Hazar catchement
Kurk River
landslide scarps
20°
30°
40°
EURASIA
20mm/year
NAF
ANATOLIA
EAF
ARABIA
Dead Sea Fault

F

61

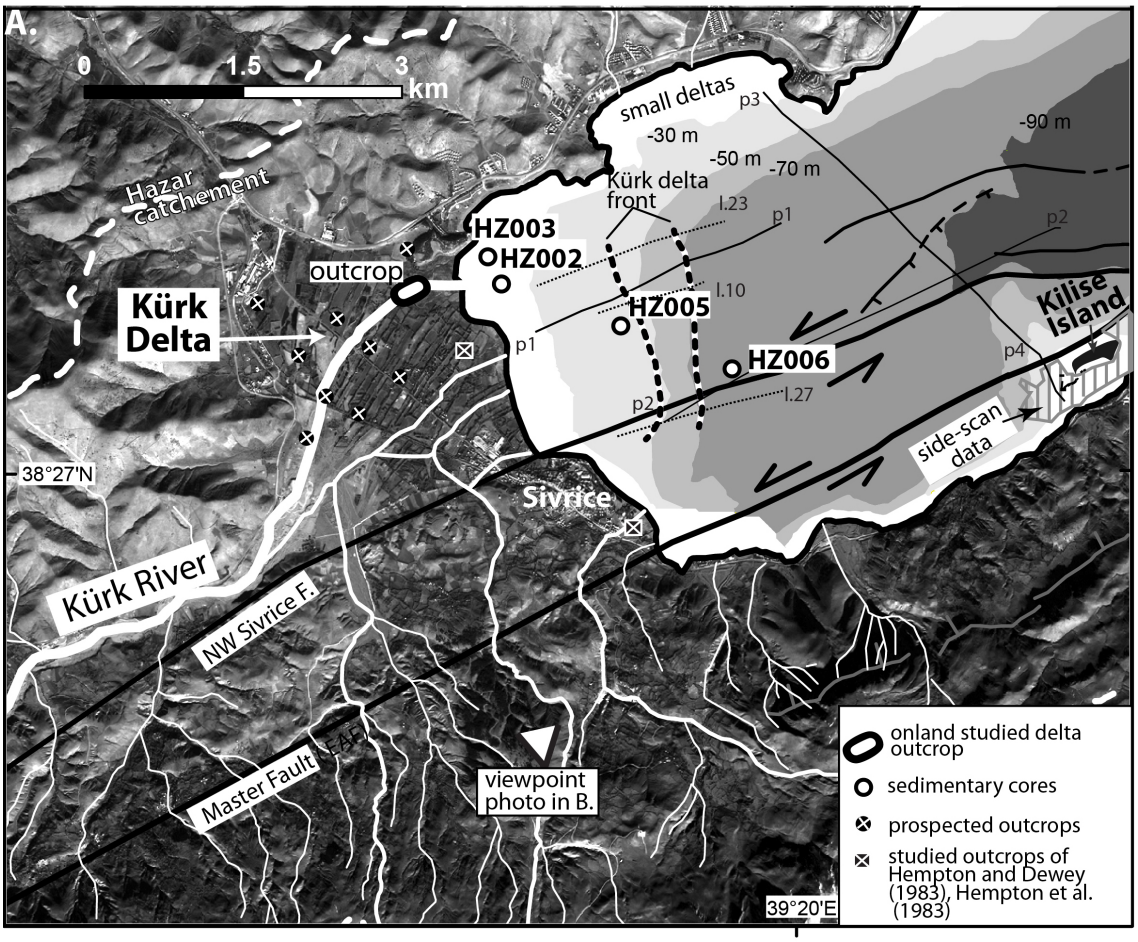
A.
0
1.5
3
km
Hazar catchement
Kürk Delta
outcrop
HZ003
HZ002
HZ005
HZ006
small deltas
p3
-30 m
-50 m
-70 m
-90 m
Kürk delta front
l.23
p1
p2
l.10
p1
p2
l.27
p4
Kilise Island
side-scan data
38°27'N
Sivrice
Kürk River
NW Sivrice F.
Master Fault
viewpoint photo in B.
39°20'E
onland studied delta outcrop
sedimentary cores
prospected outcrops
studied outcrops of Hempton and Dewey (1983), Hempton et al. (1983)


B
WSW
ENE
Kürk Delta
Sivrice

Figure 3.

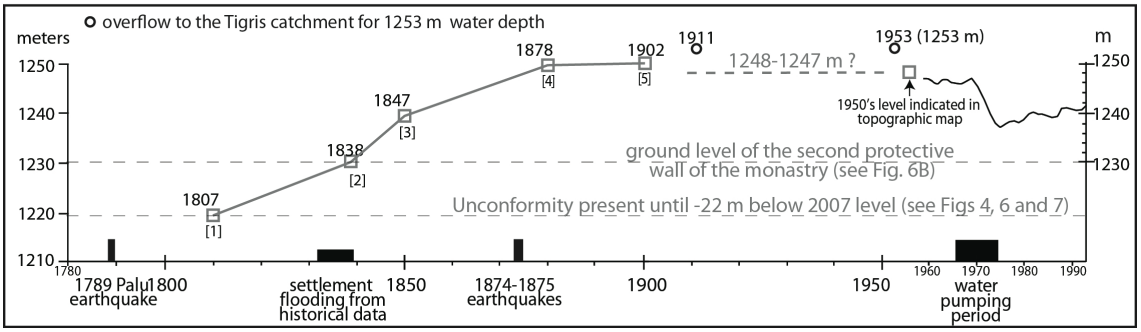
overflow to the Tigris catchment for 1253 m water depth
meters
m
1250
1240
1230
1220
1210
1807
[1]
1838
[2]
1847
[3]
1878
[4]
1902
[5]
1911
1953 (1253 m)
1248-1247 m ?
1950's level indicated in topographic map
ground level of the second protective wall of the monastry (see Fig. 6B)
Unconformity present until -22 m below 2007 level (see Figs 4, 6 and 7)
1780
1789 Palu earthquake
1800
settlement flooding from historical data
1850
1874-1875 earthquakes
1900
1950
1960
1970
water pumping period
1980
1990

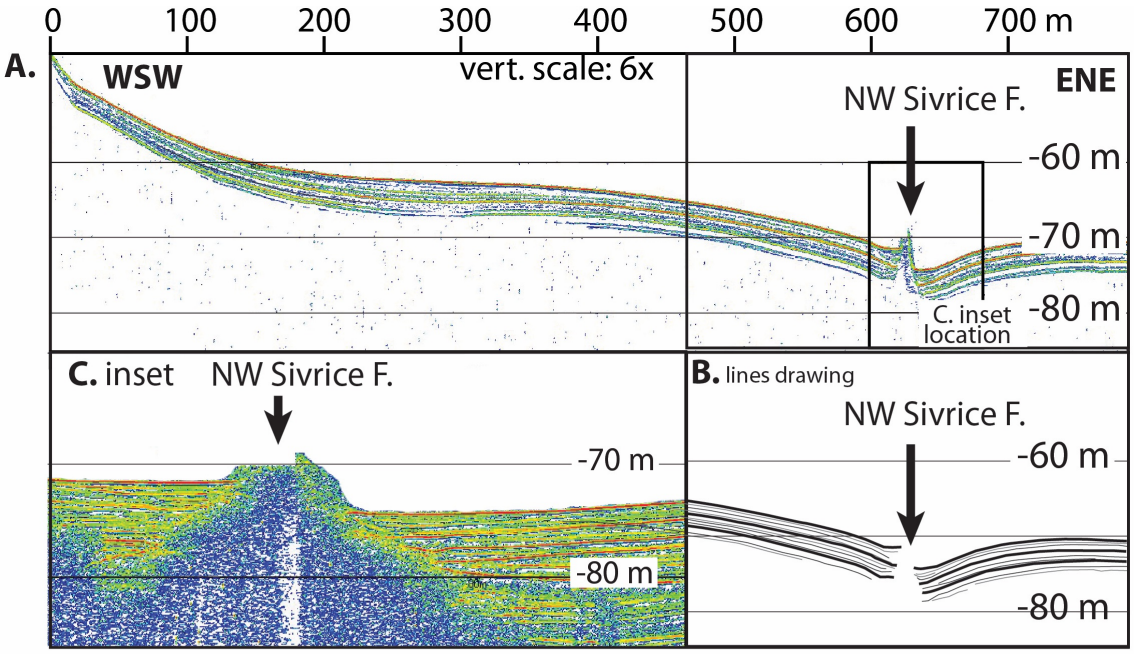
0
100
200
300
400
500
600
700 m
A.
WSW
vert. scale: 6x
ENE
NW Sivrice F.
-60 m
-70 m
-80 m
C. inset location
C. inset
NW Sivrice F.
-70 m
-80 m
B. lines drawing
NW Sivrice F.
-60 m
-80 m

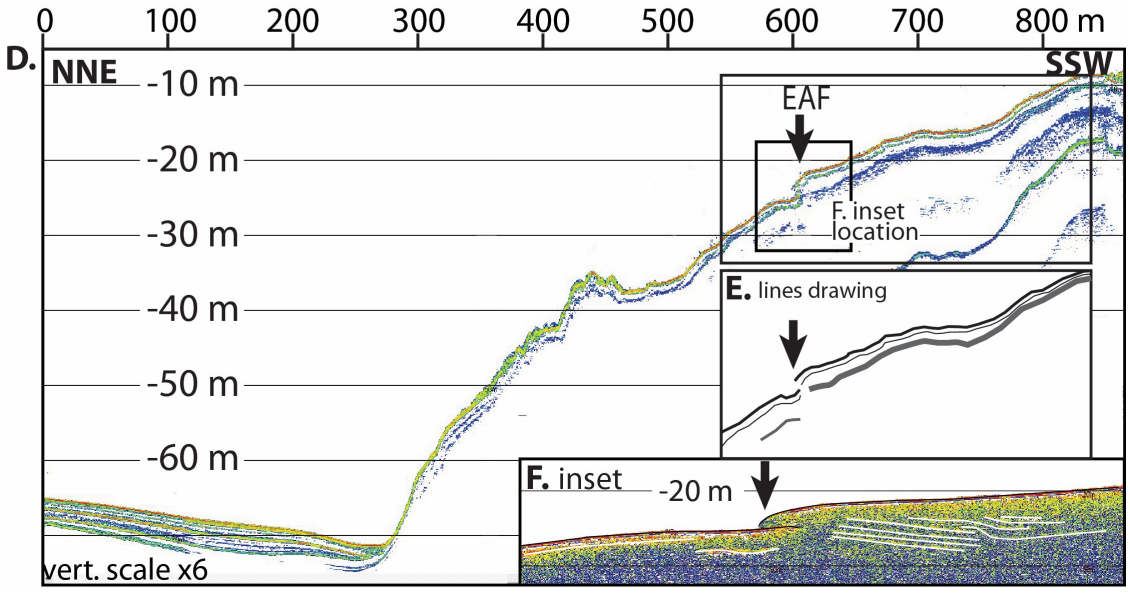
0
100
200
300
400
500
600
700
800 m
D.
NNE
SSW
-10 m
-20 m
-30 m
-40 m
-50 m
-60 m
EAF
F. inset location
E. lines drawing
F. inset
-20 m
vert. scale x6

Figure 5

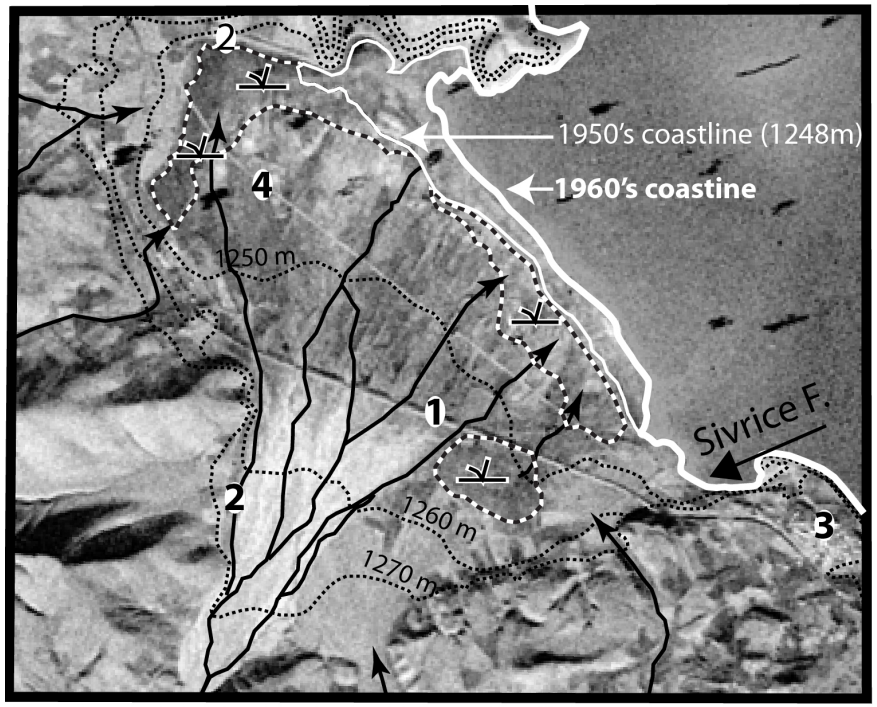

1: railroad built in the 1930's; 2: dirt road improved after 1955; 3: Sivrice town; 4: road constructed after 1955. Swampy areas (⊻) in 1955 are circled by thick dash lines.

4: enlarged roads; 5: expansion of the Sivrice Town; 6: Industrial sites

◇ outcrop studied

Hempton et al. (1983) 's outcrop

lake levels in 1950's and in 1960 (see left image)

65

Figure 6.

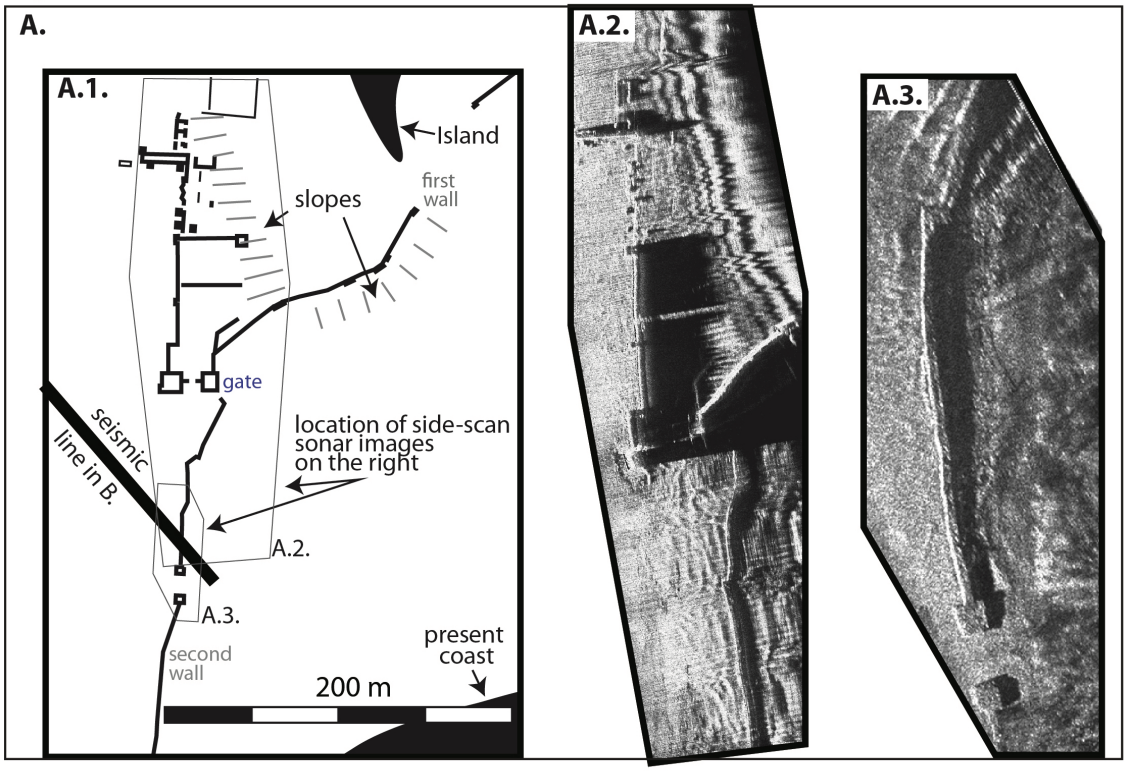
A.
A.1.
Island
slopes
first wall
gate
seismic line in B.
location of side-scan sonar images on the right
A.2.
A.3.
second wall
present coast
200 m
A.2.
A.3.

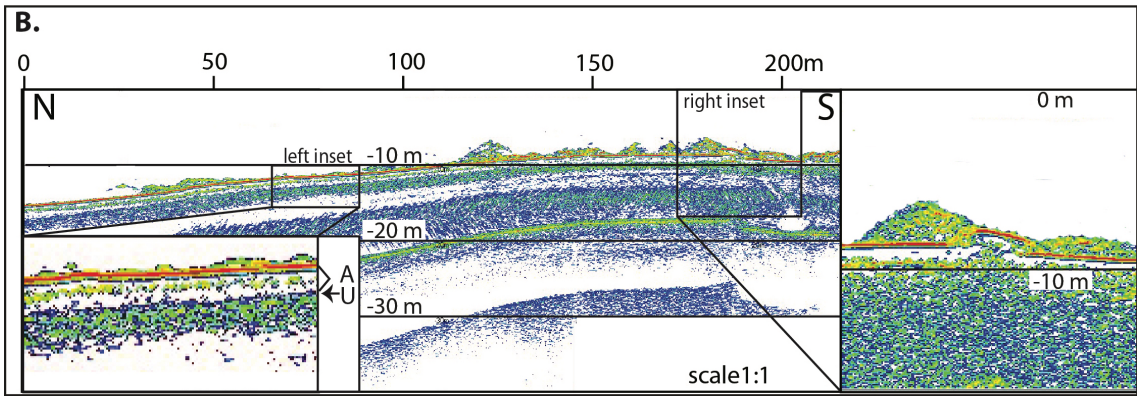
B.
0
50
100
150
200m
N
S
right inset
left inset
-10 m
-20 m
-30 m
A
U
0 m
-10 m
scale1:1

Figure 7.

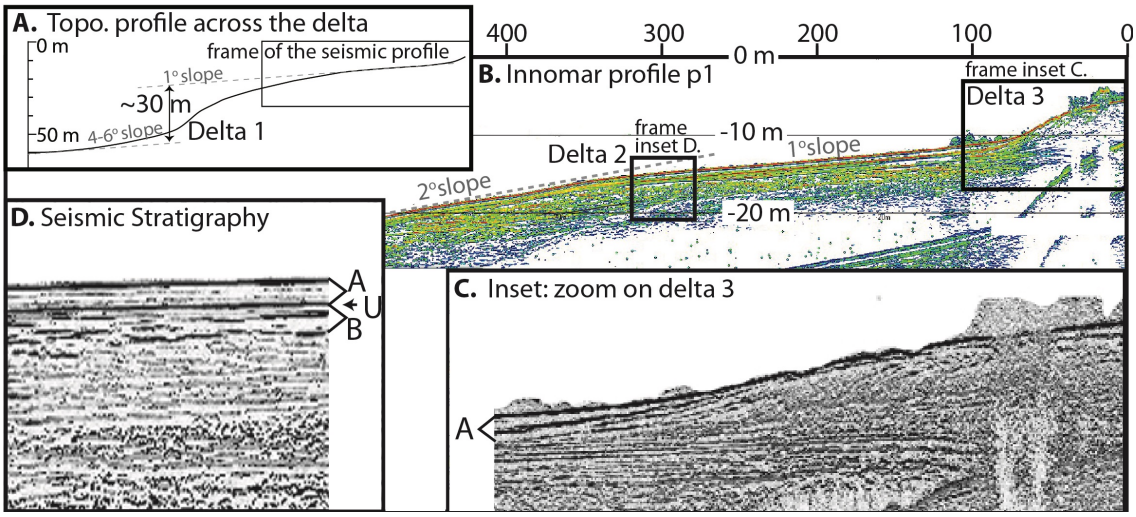
A. Topo. profile across the delta
0 m
frame of the seismic profile
1° slope
~30 m
50 m
4-6° slope
Delta 1
400
300
200
100
0
0 m
B. Innomar profile p1
frame inset C.
Delta 3
frame inset D.
-10 m
Delta 2
1°slope
2°slope
-20 m
D. Seismic Stratigraphy
A
U
B
C. Inset: zoom on delta 3
A

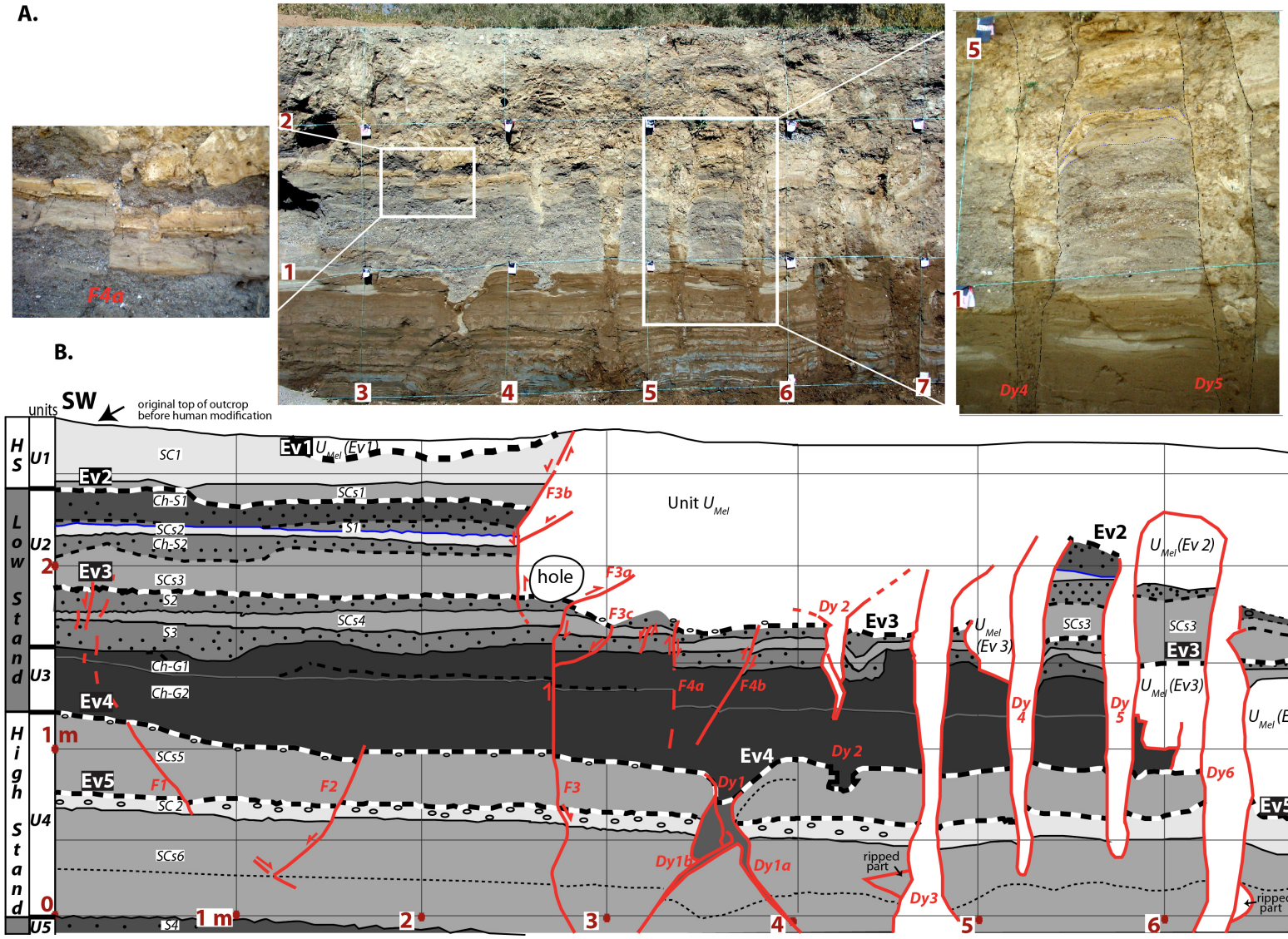
A.
F4a
1
2
3
4
5
6
7
Dy4
Dy5
B.
units
SW
original top of outcrop
before human modification
NE
Hs
Low Stand
High Stand
U1
U2
U3
U4
U5
Ev1
Ev2
Ev3
Ev4
Ev5
SC1
SCs1
SCs2
SCs3
SCs4
SCs5
SCs6
S1
S2
S3
S4
Ch-S1
Ch-S2
Ch-G1
Ch-G2
SC 2
Unit U Mel
hole
F1
F2
F3
F3a
F3b
F3c
F4a
F4b
Dy 1
Dy 2
Dy1a
Dy1b
Dy3
Dy 4
Dy 5
Dy6
Dy7
U Mel (Ev1)
U Mel (Ev 2)
U Mel (Ev 3)
U Mel (Ev3)
U Mel (Ev4-5)
ripped part
1 m
1 m
0

68

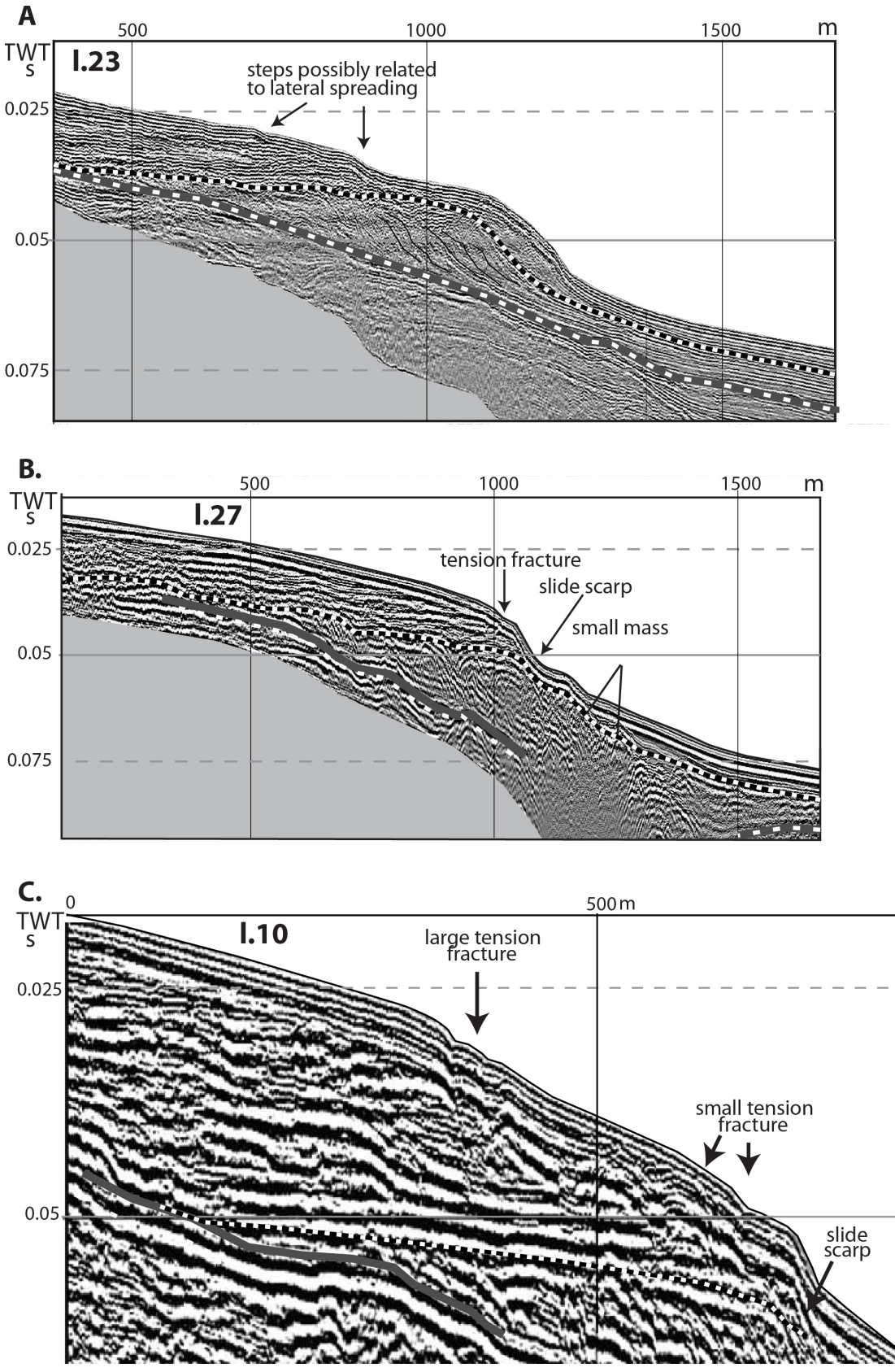
A
500
1000
1500
m
TWT
s
l.23
steps possibly related
to lateral spreading
0.025
0.05
0.075
B.
500
1000
1500
m
TWT
s
l.27
tension fracture
slide scarp
small mass
0.025
0.05
0.075
C.
0
500 m
TWT
s
l.10
large tension
fracture
small tension
fracture
slide
scarp
0.025
0.05

Figure 10.

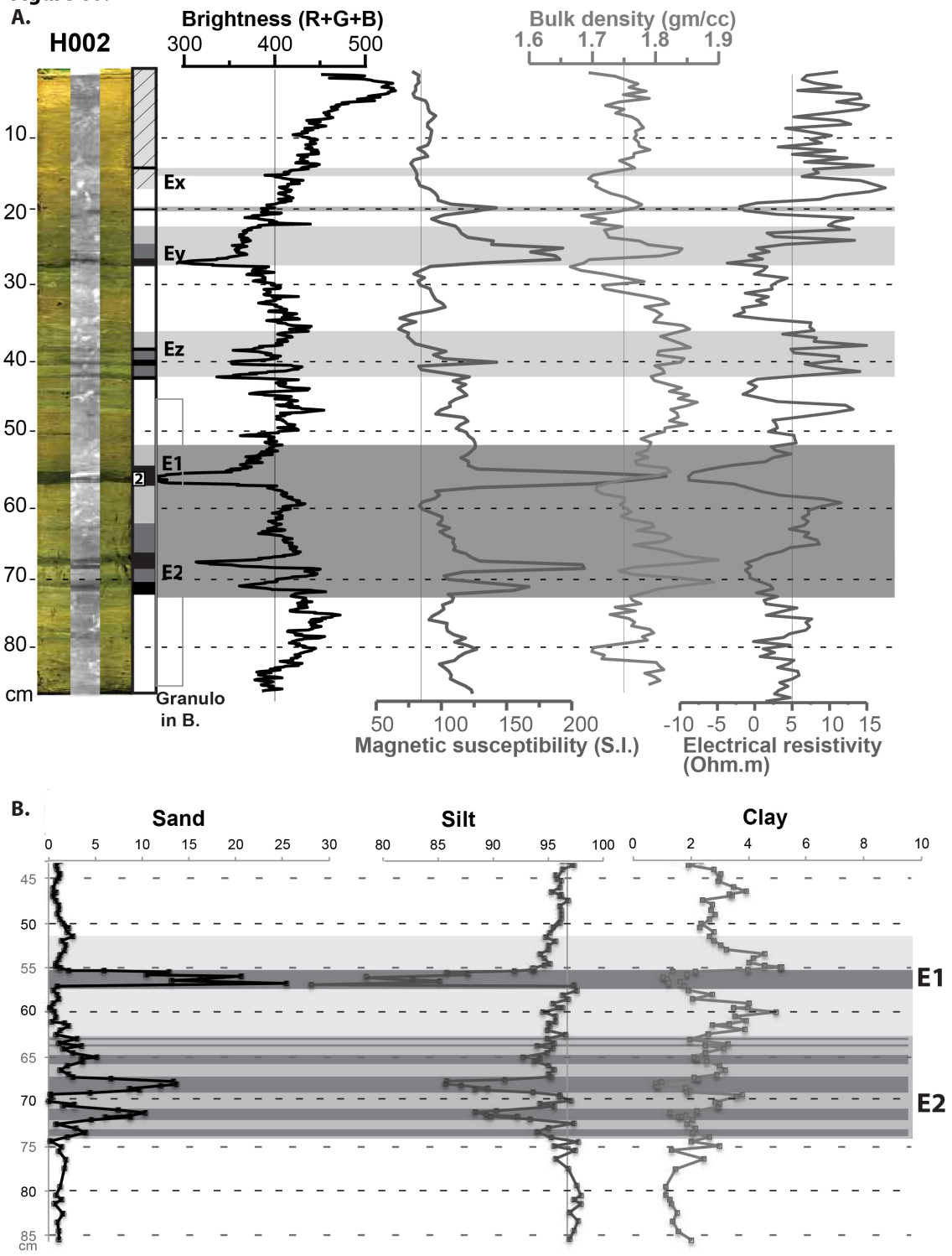
A.
H002
Brightness (R+G+B)
300 400 500
Bulk density (gm/cc)
1.6 1.7 1.8 1.9
10
20
30
40
50
60
70
80
cm
Ex
Ey
Ez
E1
E2
2
Granulo
in B.
50 100 150 200
Magnetic susceptibility (S.I.)
-10 -5 0 5 10 15
Electrical resistivity
(Ohm.m)
B.
Sand
0 5 10 15 20 25 30
Silt
80 85 90 95 100
Clay
0 2 4 6 8 10
45
50
55
60
65
70
75
80
85
cm
E1
E2

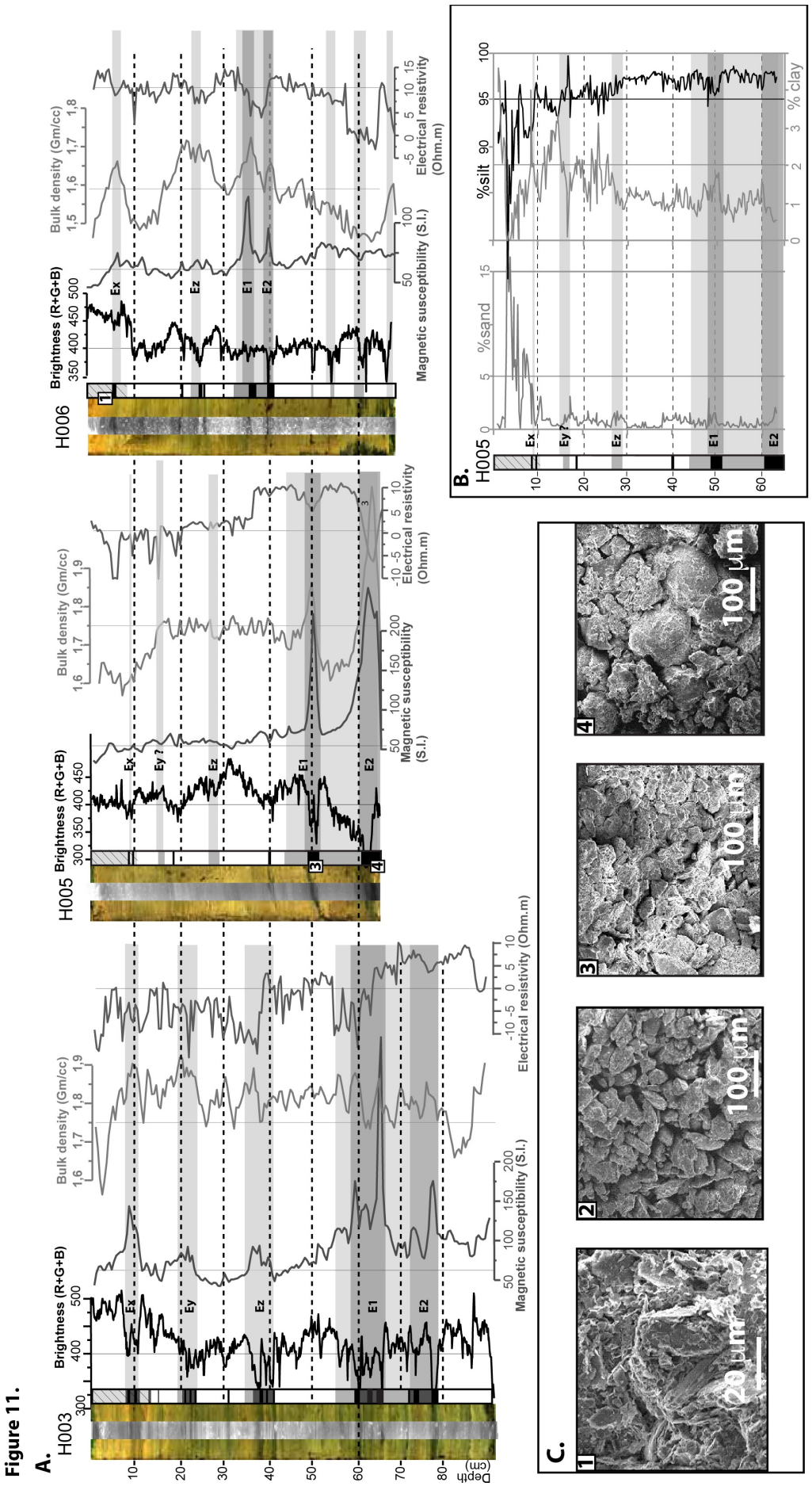
A.
H003
H005
H006
Brightness (R+G+B)
Bulk density (Gm/cc)
Magnetic susceptibility (S.I.)
Electrical resistivity (Ohm.m)
Depth (cm)
Ex
Ey
Ey ?
Ez
E1
E2
B.
%silt
%sand
% clay
C.
20 µm
100 µm

Figure 11.

Figure 12.

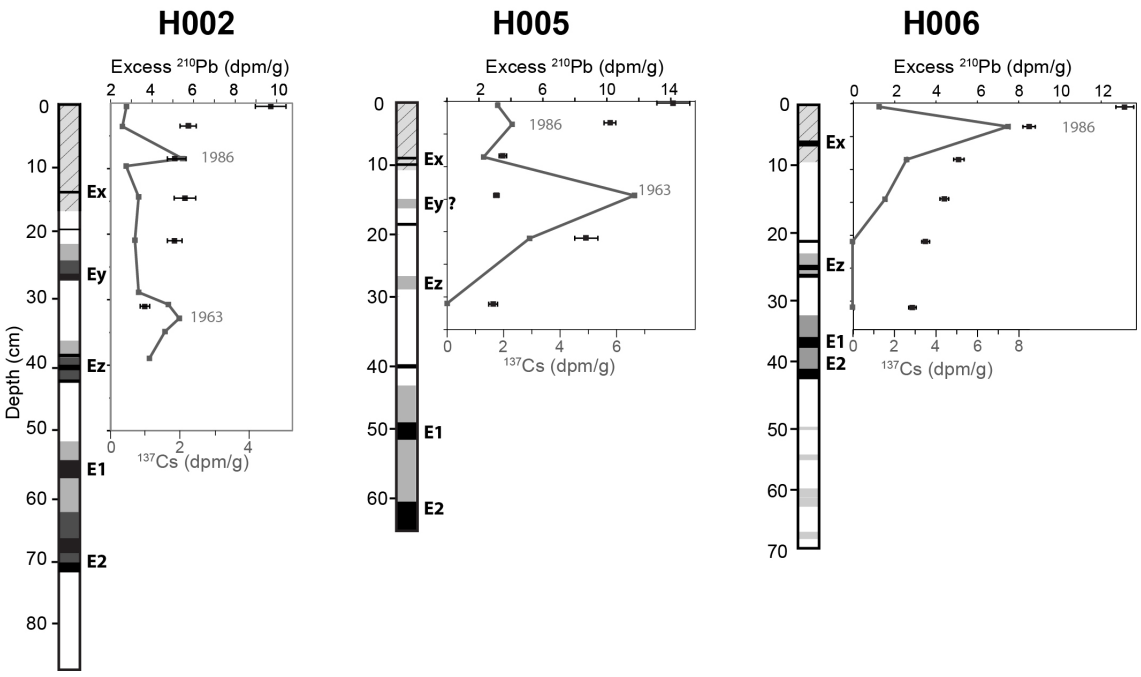
H002
H005
H006
Excess ^{210}Pb (dpm/g)
^{137}Cs (dpm/g)
Depth (cm)
1986
1963
Ex
Ey
Ey?
Ez
E1
E2

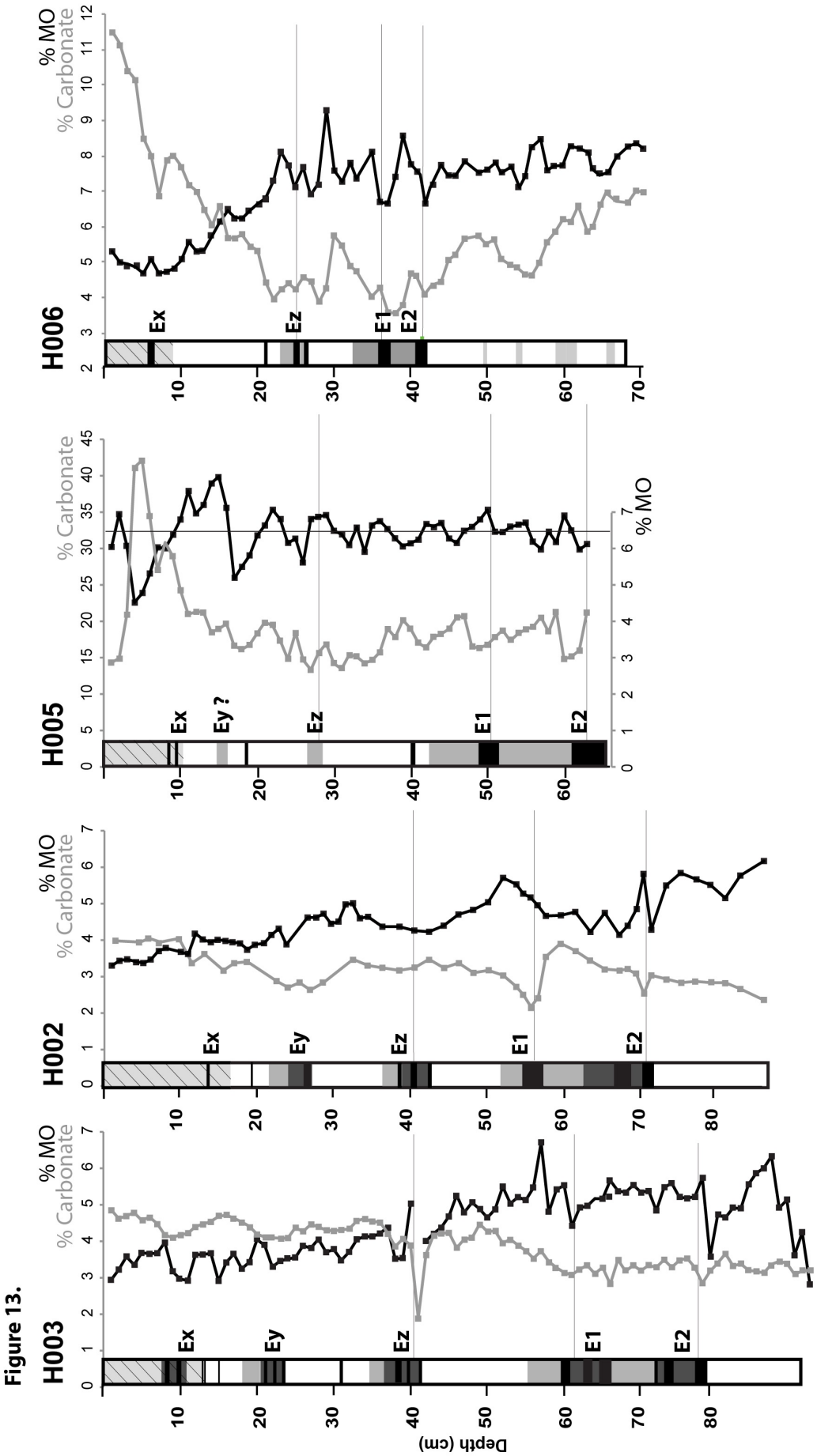
H006
% MO
% Carbonate
Ex
Ez
E1
E2
H005
% Carbonate
% MO
Ex
Ey ?
Ez
E1
E2
H002
% MO
% Carbonate
Ex
Ey
Ez
E1
E2
H003
% MO
% Carbonate
Ex
Ey
Ez
E1
E2
Depth (cm)

Figure 13.

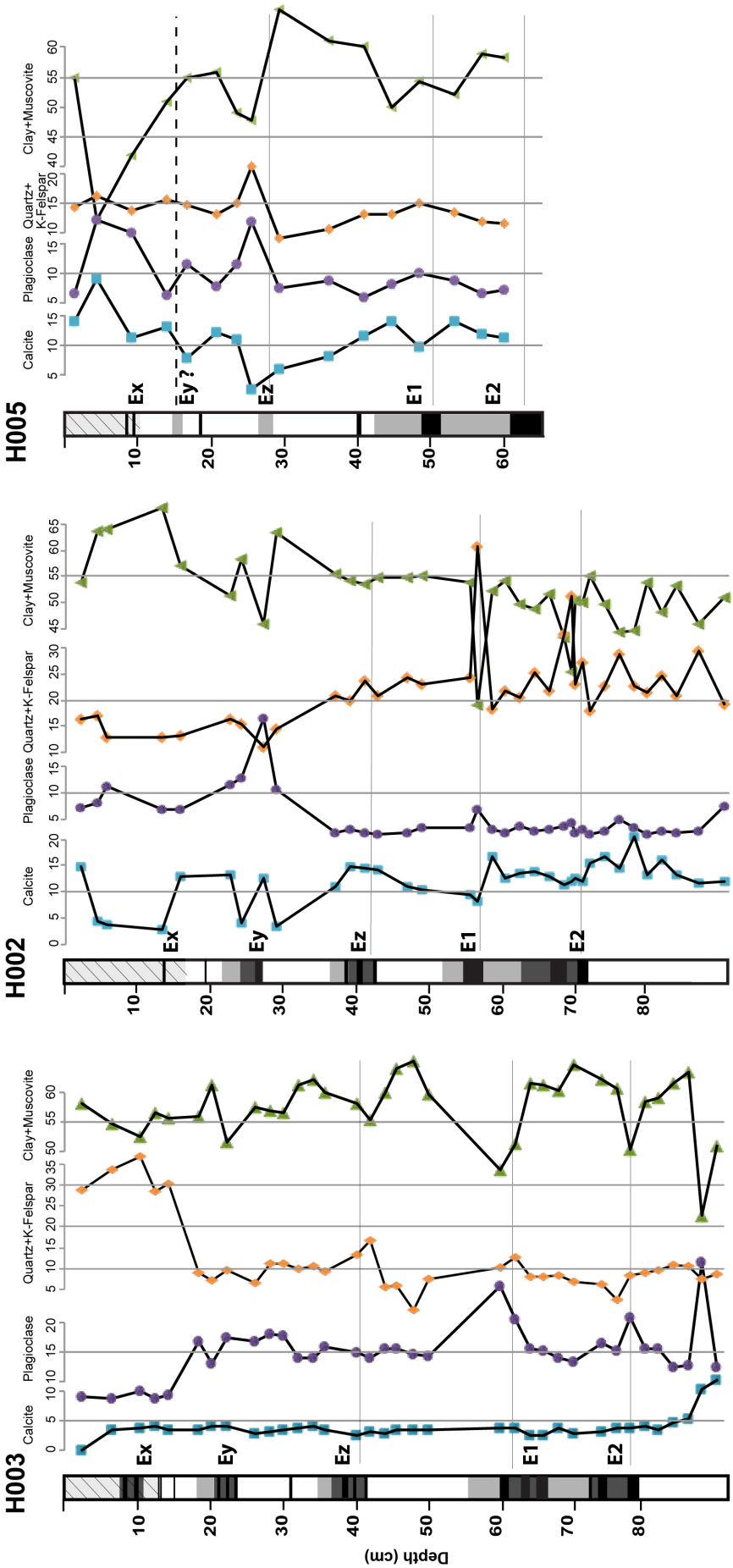
H005
H002
H003
Calcite
Plagioclase
Quartz+K-Felspar
Clay+Muscovite
Ex
Ey ?
Ey
Ez
E1
E2
Depth (cm)

Figure 15.

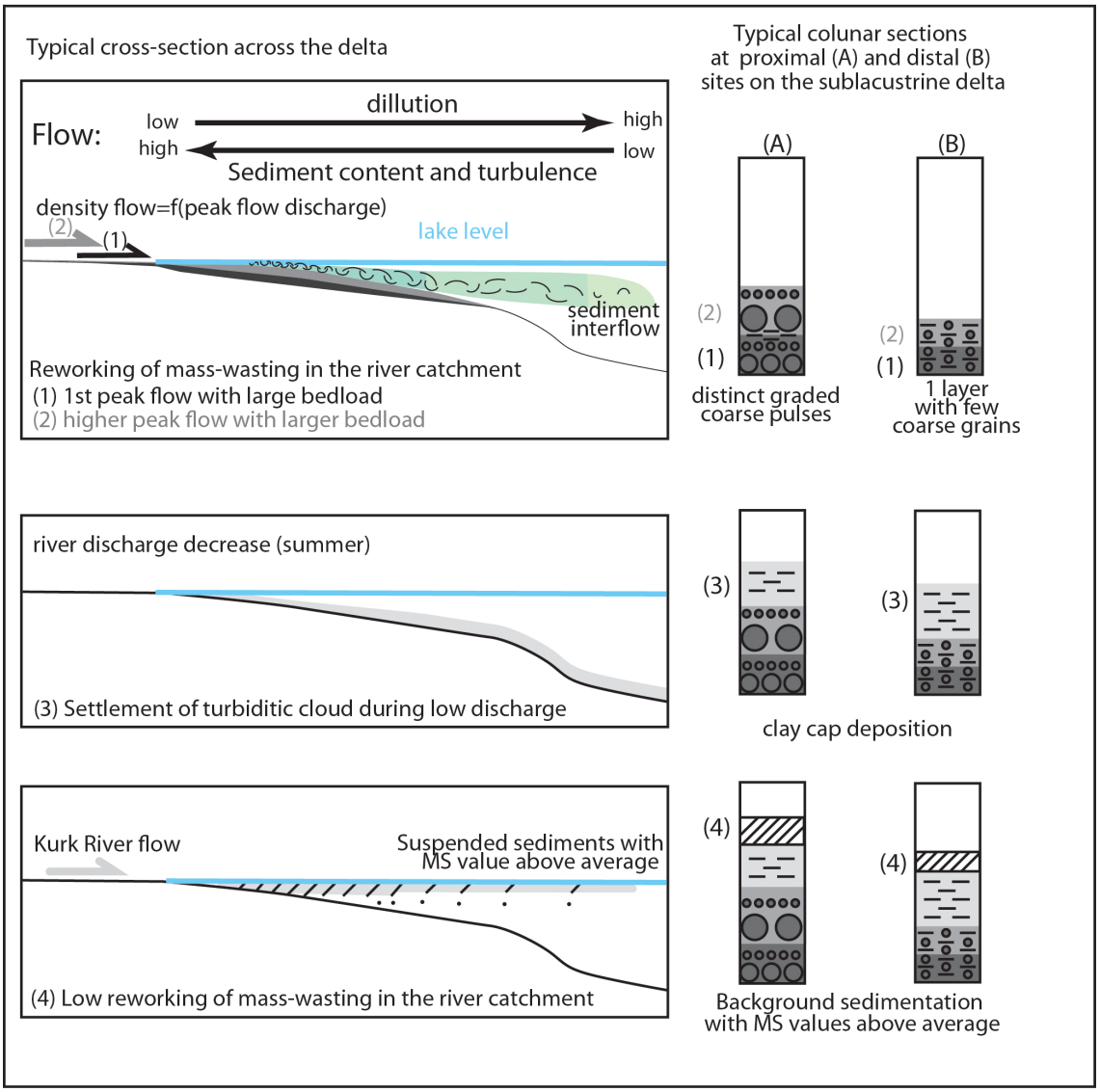
Typical cross-section across the delta
Flow:
low
high
dillution
high
low
Sediment content and turbulence
density flow=f(peak flow discharge)
(2)
(1)
lake level
sediment
interflow
Reworking of mass-wasting in the river catchment
(1) 1st peak flow with large bedload
(2) higher peak flow with larger bedload
Typical colunar sections
at proximal (A) and distal (B)
sites on the sublacustrine delta
(A)
(B)
(2)
(1)
distinct graded
coarse pulses
(2)
(1)
1 layer
with few
coarse grains
river discharge decrease (summer)
(3) Settlement of turbiditic cloud during low discharge
(3)
(3)
clay cap deposition
Kurk River flow
Suspended sediments with
MS value above average
(4) Low reworking of mass-wasting in the river catchment
(4)
(4)
Background sedimentation
with MS values above average